Graphene and Graphene-like Two-Dimensional Materials in Photodetection: Mechanisms and Methodology

Zhenhua Sun[†,‡,§] and Haixin Chang[†,⊥,*]

[†]State Key Laboratory of Material Processing and Die & Mold Technology, School of Materials Science and Engineering, Huazhong University of Science and Technology (HUST), Wuhan 430074, China, [‡]Laboratoire de Physique et d'Etude des Matériaux, PSL Research University, ESPCI-ParisTech, 10 rue Vauquelin, F-75231 Paris Cedex 5, France, [§]CNRS, UMR 8213, F-75005 Paris, France, and [⊥]WPI-Advanced Institute for Materials Research, Tohoku University, Sendai 980-8577, Japan

ABSTRACT Graphene and graphene-like two-dimensional (2D) materials have attracted much attention due to its extraordinary electronic and optical properties, which accommodate a large potential in optoelectronic applications such as photodetection. However, although much progress has been made, many challenges exist in fundamental and practical aspects hindering graphene and graphene-like 2D materials from photodetector and other photonic and optoelectronic applications. Here, we review the recent progress in photodetection based on graphene and graphene-like 2D materials and start with the summary of some most important physical mechanisms, including photoelectric, photo-thermoelectric, and photo-bolometric regimes. Then methodology-level discussions are given from viewpoints of state-of-the-art designs in device geometry and materials. It is worth emphasizing that emerging photodetection and photodetectors based on graphene-like 2D materials such as metal chalcogenide nanosheets are reviewed systematically. Finally, we conclude this review in a brief discussion with remaining challenges in photodetection of two-dimensional photonics and optoelectronics (2D POE) and note that complete understandings of 2D materials and 2D POE may inspire solar energy conversion and other new applications.

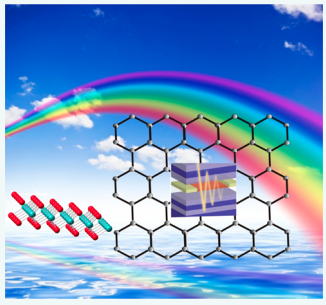

KEYWORDS: graphene · graphene-like two-dimensional materials · photodetection · photodetector · mechanism · methodology · device geometry · materials engineering · two-dimensional photonics and optoelectronics

Graphene is a monatomic-thick 2D material with carbon atoms arranged in hexagonal honeycomb lattice and has numerous attractive electronic, optical, mechanical, and thermal properties.[1,2] Electrons propagating in graphene behave as massless Dirac fermions with linear relationship between energy and momentum. This gives graphene extremely high charge carriers mobility up to 10^5 cm^2/Vs at ambient temperature and 10^6 cm^2/Vs at low temperatures.[3,4] This excellent electronic property has aroused wide interests to apply graphene in high-frequency and high-speed electronic devices such as field-effect transistors and inverters, and graphene has been increasingly deemed as an alternative material of performance-exhausting silicon.[4] However, the zero band gap and semimetal features of graphene hinder its application in logic switching devices.[5] This "drawback", on the other hand, is promising for optoelectronic application because it breaks the "long wavelength limit" of other semiconductors which are transparent to the light with photon energy smaller than their band gaps. Moreover, single-layer graphene shows high optical absorption coefficient of 7×10^5 cm^{-1} over a wide range from 300 to 2500 nm, which is much higher than conventional semiconductor materials.[6] These excellent optical properties, combined with the high Young's modulus (up to ~1 TPa for defect-free graphene) and thermal conductivity (up to ~5000 W/mK for suspended single-layer graphene at room temperature), offer promising prospect of graphene as supporting and/or active materials in a variety of functional devices such as light-emitting diodes, solar cells, photocatalysts, biosensors, and photodetectors.[7−10] In addition to graphene, very recently, other 2D materials, usually indicated by graphene-like

* Address correspondence to hxchang@hust.edu.cn, hxchang@wpi-aimr.tohoku.ac.jp.

Received for review January 25, 2014 and accepted April 9, 2014.

Published online April 09, 2014
10.1021/nn500508c

2D materials, are also emerging as important alternatives to graphene in electronics and optoelectronics.[11−17] Graphene-like 2D materials, such as layered transition metal dichalcogenides (TMD), metal oxides, and boron nitride (h-BN) nanosheets, have two-dimensional structures similar to graphene but very different electronic and optical properties. Graphene-like 2D materials can be semiconductor, insulator, metal, or superconductor and paramagnetic, diamagnetic, anti-ferromagnetic, or ferromagnetic depending on the composition and phases.[11−18] Graphene and graphene-like 2D materials therefore provide facile and versatile platforms for various applications.

Photodetection and photodetectors have significant importance in modern society from practical aspects like imaging, communication devices, various sensors for safety monitoring, and display technology to fundamental science applications such as observing the universe.[19−24] Photodetection is a process converting light signals to electric signals, amid which three physical mechanisms are involved in sequence: light harvesting, exciton separation, and charge carrier transport to respective electrodes. The efficiency of light energy utilization can be described by external quantum efficiency (EQE):

$$EQE = \frac{I_{ph}}{q\phi} = \frac{h\nu}{q}\frac{I_{ph}}{P} \quad (1)$$

where I_{ph} is the photocurrent, defined as the discrepancy between current under illumination and in dark; ϕ is the photon flux, defined as the number of incident photons; q is the unit electron charge; $h\nu$ is the energy of one single photon; P is the power of incident light.[24] Particularly, one commonly used figure of merit representative of photoresponse ability is the responsivity, which is defined as

$$R = \frac{I_{ph}}{P} = EQE\frac{q}{h\nu} \quad (2)$$

where R has the unit of A/W.[24] Another important figure of merit is the detectivity, which represents the ability to detect signal from noise and is defined as

$$D = \frac{I_{ph}}{p\sqrt{2qI_{dark}}} \quad (3)$$

where p is light intensity and I_{dark} is the dark current.[21] When an illumination is shed on a photodetector, the photocurrent will change until saturation. The time used for this process is called response time t. Some papers used the time that photocurrent attained certain percentage of saturated one to define the response time.[22,23] Photodetectors can be divided, in general, into two categories conceptually: photoconductors and photodiodes. The former one refers to the overall conductivity change of materials sandwiched between two electrodes, and the latter one invokes the behavior dependence of p−n or Schottky junctions on light illumination.[20,24] For photodiodes, the EQE is normally less than 1, due to the insufficient absorption of light, carrier recombination, and other reasons, but the response will be fast because both electrons and holes are involved in the photocurrent generation and they recombine after reaching to their own electrodes with short carrier lifetime. On the contrary, only one type of carrier contributes to the photocurrent with the other one trapped in a photoconductor. The transporting carriers can circulate many times before recombining with their counterpart, leading to an internal gain and EQE larger than 1 with high responsivity but long response time. Photodetectors based on silicon are limited to the visible region due to its band gap of 1.4 eV, corresponding to wavelength of ∼900 nm. Long wavelength photodetector products in the market based on crystalline InGeAs/HgCdTe suffer from either expensive fabricating process (*e.g.*, molecular beam epitaxy) or rigorous operation demands (*e.g.*, low temperature), sometimes both. In contrast, graphene possesses many natural virtues and has become more and more attractive with remarkable progress in the low-cost, large-scale, high-quality growth and the facile manipulation of electronic and optoelectronic properties.[6,19,20]

It is worth noting that, despite the high absorption coefficient, due to the short interaction length, single-layer graphene absorbs only ∼2.3% in visible and infrared regions. This value is insufficient for photodetection application, although it is remarkable for a single-atom-thick membrane. The zero band gap indeed makes graphene a promising candidate for broadband detection even at terahertz and infrared region,[25] while on the other hand, it leads to short lifetime of exciton in pure graphene which is unfavorable for the exciton separation and high photoresponsivity.[6,26,27] The high, ambipolar charge carrier mobility in single-layer graphene supports high-speed

VOCABULARY: **graphene-like 2D materials** - two-dimensional materials sharing similar structure with graphene but with different compositions, in which atoms arrange in two dimensions with much stronger bond strength than a third dimension; **materials engineering** - modifying the shape, composition, and other structural properties of materials for specific functionality; **two-dimensional photonics and optoelectronics** - photonics and optoelectronics in two-dimensional materials; **phototransistor** - a transistor for photodetection purpose; **responsivity** - the ability of a photodetector to sense illumination, with a unit of "ampere per watt", equal to "photoresponsivity" herein; **detectivity** - the ability of a photodetector to distinguish photoresponse signal from nosie, equal to "photodetectivity" herein; **photoelectric effect** - photons excite electrons to high energy level charge carriers for electric current; **photo-thermoelectric effect** - light illuminations generate temperature discrepancy across the active area which will induce electric current signal; **photo-bolometric effect** - light illuminations generate temperature change of active materials which will induce resistance change consequently.

devices firmly but with the cost of low light absorption.[2,28] Thus, the responsivity of photodetectors based on pure single-layer graphene is limited to ~6.1 mA/W.[29] Many efforts have been devoted to the improvement of photodetection devices based on graphene materials. One strategy is to functionalize graphene through materials engineering such as creating a band gap in graphene by doping,[30,31] shaping graphene to nanoribbons,[32,33] using reduced graphene oxide,[34−36] applying vertical bias,[37,38] and so on. Another strategy is to deliberately design device structure, for instance, integrating graphene materials with optical structures such as plasmonic structure,[39−43] optical waveguide,[44−48] and optical cavity[49−52] to increase the light−graphene interaction and light absorption. Making use of the intrinsic plasmonic effect of graphene by patterning graphene into nanostructure may pave another way toward high-performance photodetection devices.[53] The third strategy is to combine graphene with various materials such as polymers, nanoparticles, quantum dots, and thin film to form hybrids.[21−23,54−71] These additives can not only serve as light harvesters but also render interfaces and junctions facilitating exciton separation. These strategies and methods have involved diverse and ingenious designs in both functionalities of materials and device geometry. Very recently, inspired by the success of graphene in photodetection, graphene-like 2D materials such as metal chalcogenide nanosheets are also widely studied to explore the performance in photodetection.[72−82] Although it is still in infancy, some intriguing achievements have been obtained in improving responsivity.

However, although much progress has been made, especially for graphene, many challenges exist in fundamental and practical aspects hindering graphene and graphene-like 2D materials from photodetector and other optoelectronic applications. The physical mechanisms of photoresponse in photonic and optoelectronic devices are still controversial to date. One or several mechanisms including photoelectric,[23,26,29,83−89] photothermoelectric,[89−97] and photo-bolometric[98−101] mechanisms may be included in the devices. Moreover, despite many functional methods having been applied, there is no comprehensive overview in methodology level for the optimization of photodetectors based on 2D materials. Herein, we will review the recent progress in photodetection based on graphene and graphene-like 2D materials and start with the summary of some most important physical mechanisms. Then methodology-level discussions are given from viewpoints of state-of-the-art designs in device geometry and materials. It is worth emphasizing that emerging photodetection and photodetectors based on graphene-like 2D materials such as metal chalcogenide nanosheets are reviewed systematically. Finally, we conclude this review in a brief discussion with the remaining challenges in the photodetection of two-dimensional photonics and optoelectronics (2D POE) and note that the complete understanding of 2D materials and 2D POE may inspire solar energy conversion and other new applications.

Physical Mechanisms in the Photodetection Process of Graphene and Graphene-like 2D Materials. We will discuss three most important physical mechanisms in the photodetection of 2D materials including photoelectric, photothermoelectric, and photo-bolometric effects. Other mechanisms may also be applied in photodetection especially for hybrids and heterostructures such as photoinduced charge transfer or tunneling, photogating and field effect doping.[9,23,58,59,61] We just mention these mechanisms without further discussion because the hybrid components, instead of 2D materials, are the main contribution of photoresponses in most of situations.

Photoelectric Effect. Graphene is more suitable for photoconductor geometry for its two-dimensional atomic structures. Thus, so far, almost all graphene photodetection devices are fabricated with graphene longitudinally aligning between two electrodes. In the graphene channel, incident photons excite electrons to form excitons which then are separated and propelled by the external bias to form a photocurrent. Nevertheless, for the unique electronic properties of graphene, graphene devices show different features from conventional semiconductors. Two regions can be divided geographically, the area around the graphene−metal junction and the area far away from it. Regarding the latter region, photoconductive (PC) effect dominates its photoresponse, with graphene playing the classic role of conventional semiconductors in photoconductors.[24,100] The photocurrent can be described as

$$I_{ph} = AVq\mu\Delta n \quad (4)$$

where A is the cross section area of the active layer; V is the applied bias; q is the unit electron charge, μ is the charge carrier mobility; Δn is the photoinduced carriers density. Apparently, the high carrier mobility of graphene is its remarkable advantage for the photodetecton application. On the other hand, as aforementioned, due to the low absorption and short lifetime of photon-induced carriers in graphene which is below tens of picoseconds before recombination,[26,88,102,103] the internal quantum efficiency will be too low to support the photoresponse performance demanded. Many efforts have been undertaken to improve the photoresponse from this part, which will be demonstrated in the following section.

Further study unveiled that, unlike the pure graphene region where intrinsic photoexcitation happens, the metal electrode−graphene junction plays a substantial role with its photovoltaic trait in the photoresponse process of graphene devices.[83−89] Therefore, this type of photodetection mechanism is also called the photovoltaic (PV) effect. Giovannetti *et al.* reported their study on the doping effect upon graphene by metal contacts.[104] They found that, under intimate contact between graphene and metal, the Fermi level

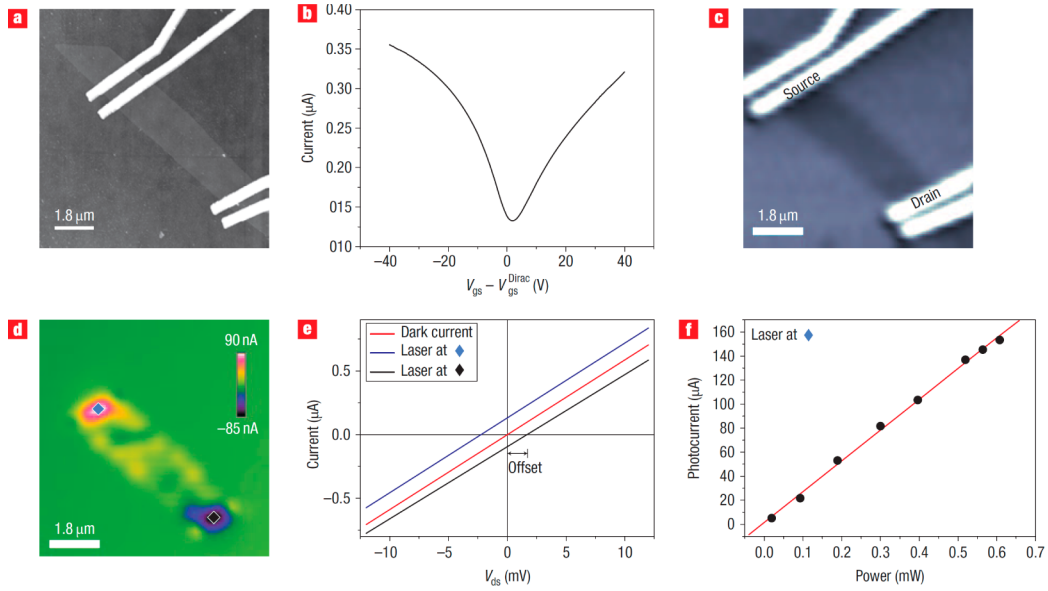

Figure 1. Photocurrent responses of a graphene device. (a) AFM image of a graphene monolayer contacted by four gold electrodes. (b) Gate dependence of the drain current (I_D) measured at V_{DS} = 1 mV. (c) Optical reflection image acquired simultaneously with the photocurrent image. The drain and source electrodes used in the measurements are indicated. (d) Photocurrent image taken at $V_{DS} = V_{GS} = 0$ V. Further measurements were performed by fixing the laser spot at the positions marked by the black and blue diamonds. (e) I_D−V_{DS} characteristics recorded in the dark and with the laser positioned as marked in (d). (f) Photocurrent detected at the position marked by the blue diamond as a function of the laser power. Reproduced from ref 83. Copyright 2010 American Chemical Society.

of graphene can be shifted either upward or downward according to the different working functions of the metal counterparts. The doping effect is remarkable because the density of states (DOS) in the vicinity of the Dirac point is low due to the linear energy-momentum relationship in graphene. It is worth noting that they further clarified the dependence of doping effects on the distance between graphene and metals, although in most graphene devices the metal electrodes are deposited by physical vapor deposition methods which will definitely give extremely close contact.

Meanwhile, Lee and co-workers used scanning photocurrent microscopy to investigate the spatial differences of photoresponses of graphene devices.[83] They found that a built-in electric field was formed around the metal−graphene interfaces, which could realize the separation of excitons without an external bias. The spatially resolved photocurrent images revealed the superior photocurrent density when illumination was shed on interface areas rather than the site far from them (Figure 1), implying more efficient carrier separation in the graphene−metal interfaces. As the potential step across the interface was decided by the Fermi level of graphene and work function of metals, a gate bias perpendicular to the graphene sheet could be used to control the photoresponse by adjusting the Fermi level of graphene. In the case of Ti/Au electrodes on graphene, the built-in bias in the metal−graphene interface can be described as

$$\Delta V = \Phi_M - \Phi_G - \Delta E_F + \mathrm{sgn}(V_{GS} - V_{GS}^{Dirac})\hbar v_F \sqrt{\pi\alpha}\sqrt{V_{GS} - V_{GS}^{Dirac}} \quad (5)$$

where Φ_M and Φ_G are the work functions of metal and graphene, respectively; ΔE_F is the Fermi level shift of graphene caused by metal doping; V_{GS} is the gate bias applied; V_{GS}^{Dirac} is the gate bias under which graphene is in its charge-neutral point; α is 7.2×10^{10} cm^{-2} V^{-1}, and $\hbar v_F$ is 5.52 eVÅ.[83] Scanning photocurrent microscopy has been proven to be a powerful tool to study carrier dynamics in two-dimensional graphene-based devices. Park *et al.* probed the photocurrent generation and collection in single-layer graphene and extracted a exciton separation efficiency >30% in the graphene−metal interface junctions under illumination of 532 nm.[85] Contemporaneous works have also been done by Xia and co-workers.[84,86] Their reports, in particular, pointed out that the doping and local bias did not happen just in the graphene beneath the metal electrode but also extended 200−450 nm into the graphene channel. Using Ti/Pd/Au triple-layer metal electrodes and single-layer graphene, responsivity of 1 mA/W was obtained under a laser of 632.8 nm with 30 μW power, without external bias. This suppressed value can be ascribed to the short lifetime of carriers and low absorption of single-layer graphene as aforementioned. However, this feature is favorable for high-speed operation which needs the photocarriers to annihilate quickly after removing the radiation. Using infrared laser pulses with a wavelength of 1550 nm, Urich *et al.* conclude that the intrinsic response time of photodetectors based on monolayer graphene can be as low as 2.1 ps, which corresponds to a theoretical optical modulating operation bandwidth of ~262 GHz.[88] Xia *et al.* also studied the response speed of devices with this simple device

geometry under the same laser pulse. They found that, although the internal quantum efficiency was 6−16% and the responsivity was below 1 mA/W, this kind of device worked without external bias and showed stable photoresponse for optical modulations up to 40 GHz and theoretically may exceed 500 GHz.[26] As the photoelectric effect works based on the direct photon−electron transition and benefits from the high carrier mobility of graphene, its response speed is very fast, which is an overwhelming advantage over the other two mechanisms to be introduced below.[26,89,96,100] The PV effect supplies the possibility of energy-saving photodetectors without the presence of external bias. Even so, the responsivity of PV devices is limited, and external bias can be used to improve it efficiently.

Besides metal−graphene junction, a graphene p−n junction underlying the photoresponse of corresponding devices has been elucidated by Peters *et al.* using scanning photocurrent microscopy.[87] In their devices, graphene was partially p-doped by oxygen in ambient with the rest n-doped by poly(ethylenimine) aqueous solution. Scanning photocurrent images were obtained under laser with wavelength of 633 nm and showed that, under illumination, exceptional high photocurrent comparable with the metal site occurred with zero external bias. They attribute this photoresponse to the built-in bias formed in the p−n interfaces due to distinct Fermi levels in two sides. Moreover, the photo-thermoelectric mechanism was excluded by the discrepancy of photocurrent behavior with photo-thermoelectric mode.

Photoelectric regime is also believed to play a significant role in the photoresponse of graphene-like 2D materials such as layered metal chalcogenides. The photocurrent generation of the MoS_2 monolayer phototransistor was believed to mainly be induced by the photogenerated carriers by PC effects.[73,77] Photonic radiations increase the charge carriers in the channel which drift under an external bias. Similar regime was also applied by Liu *et al.* to explain the photoresponse in multilayer GaTe photodetectors.[80] For comb-shaped metal contacts with layered metal chalcogenides, such as MoS_2, due to the large area of metal contacts, PV effect between MoS_2 and metal junctions may also play a role, although there is no systematic study on it yet.[79]

Photo-thermoelectric Effect. Photo-thermoelectric (PTE) effect is the thermoelectric effect induced by light illumination. Basically, this mechanism is unfavorable for the photodetection application because this serpentine energy-converting process first from light to thermal energy then to electricity has laggard speed and low efficiency.[96] However, this mechanism is believed to play a substantial role in the photoresponse especially in binary structure graphene devices. Considering the small electron heat capacity and large light-induced changes in electron temperature in graphene, this mechanism may have particular interests in photodetection and other optoelectronic applications.[92,105,106]

Thermoelectric property of graphene has been studied specially[105−108] and Xu *et al.* reported their PTE devices based on single-bilayer graphene binary structure.[90] A single-layer graphene was partially covered by another single-layer graphene, thus forming a single bilayer graphene interface. Due to the higher DOS in the vicinity of the Dirac point in bilayer graphene than single layer, under the same carrier density induced by a coordinate vertical gate bias, the change of Fermi level of single-layer graphene is supposed to be larger than that of the bilayer. This difference would lead to a built-in bias from single-layer to bilayer graphene. On the other hand, the Seebeck coefficient, S, which represents thermoelectric power, is related to the DOS and Fermi level and given by

$$S = -\frac{\pi^2 k_b^2 T}{3q}\frac{1}{G}\frac{dG}{dV_{GS}}\frac{dV_{GS}}{dE}\bigg|_{E = E_F} \qquad (6)$$

where k_b is the Boltzmann constant; T is the sample temperature; q is the unit electron charge; G is the conductance; V_{GS} is the gate bias.[90] Thus, the PTE current is given by

$$I_{PTE} = \frac{S_2 - S_1}{R}\Delta T \qquad (7)$$

where R is the resistance; S_1 and S_2 are the Seebeck coefficient of two areas; ΔT is the temperature difference.[90] According to thermodynamics, hot carriers tend to diffuse from low DOS sites to high DOS sites. Namely, for instance, under large positive vertical gate bias, which will induce electron accumulation in graphene, the photocurrent should be from the single-layer part to bilayer under the illumination if the photoelectric mechanism dominates the photoresponse at the interfaces. Otherwise, the current direction will be reverse if the PTE mechanism is in charge. Their observation through photocurrent microscopy with a laser of 635 nm clearly manifested the dominant role of the PTE mechanism in their binary structure graphene device (Figure 2). Further studies corroborated this conclusion by correlating the temperature dependence of thermal conductivity and thermoelectric power. Photoresponse was found to be higher at cryogenic temperature and follows different dependence in low- and high-temperature regions.

The core kingpin of this PTE device is to form inhomogeneous thermoelectric power across the graphene channel, and controlling the layer number of graphene is not the only pathway to this target. As a vertical gate bias can be used to adjust the Fermi level of graphene, it is possible to apply more than one vertical bias on different parts of one single graphene sheet, thus realizing a thermoelectric power discrepancy. Lemme *et al.* reported their photodetection graphene

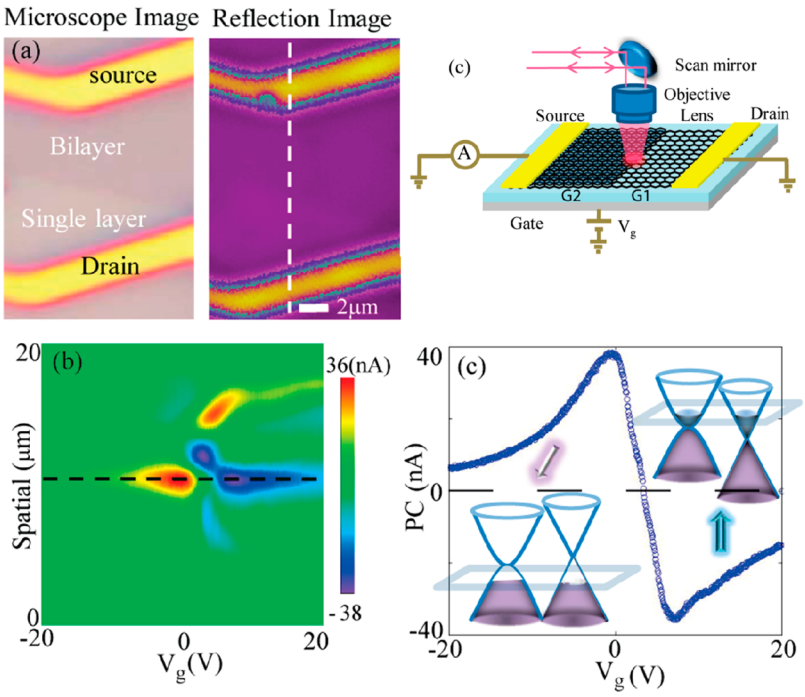

Figure 2. Device geometry, gate-bias-dependent spatial photocurrent image, and energy level for a single-bilayer graphene junction. (a) Top view image of device structure (left) and schematics (right) of the experimental setup and device geometry. (b) Photocurrent image obtained by the laser lines a a function of gate voltage, V_g. The laser scan position is indicated by the dashed white line in the reflection image in (a). (c) Photocurrent response at the center of the graphene interface junction as a function of V_g. The top right (bottom left) inset is the aligned Fermi level between the single-layer and bilayer at the n (p) doping. Reproduced from ref 90. Copyright 2009 American Chemical Society.

device with such configuration and PTE mechanism.[97] They used uniform graphene to fabricate a dual-gate graphene phototransistor and tested its photoresponse to a laser of 600 nm. The bottom gate was universal to all, and the top gate located the center of the channel. They found that between the part sandwiched between two gates and the other part affected only the by bottom gate, by adjusting carrier densities by respective gate voltages, four types of junction situations (p−n−p, p−p′−p, n−p−n, and n−n′−n) can be formed. The photocurrents across these junctions were consistent with the PTE mode. This dual-gate structure not only supplies a more controllable method to make use of PTE in graphene than material manipulation but also makes it easier to study the hot carrier transport in graphene devices. A later work reported by Gabor *et al.* got more deep insight into the role played by hot carriers in photoresponses through similar dual-gate devices.[92] The energy of photon-excited electron−hole pairs has two ways to release. The first way is energy transport through charge carriers, which may induce photocurrent, and the second is energy transfer to lattice to be heat. The second way in graphene was found to be inefficient, leading to hot carriers and cool lattice in long cooling time scales (~100 ps). These hot carriers result in nonlocal transport regime under local excitation and may be the fundamental factor of the PTE mechanism.[91,94,101]

Furthermore, the studies carried out by Song *et al.*[91] and Tielrooij *et al.*[94] unraveled another virtue of hot carriers, through measurement of photocurrent in dual-gate graphene devices and a pump−probe technique, respectively. As the carrier−carrier scattering in graphene is efficient, during the long transport length of hot carriers to contact, there is a high possibility for multiple excitations to occur. This hot-carrier-induced excitation is efficient over a wide range of light frequency and is sensitive to the doping level in graphene. It is of particular interest because higher quantum efficiency of the multiple excitations may appear when the substrate inducing higher carrier mobility in graphene was used underneath. The influence of substrates in PTE effect in graphene has been studied thereafter. Freitag *et al.* fabricated graphene phototransistors with one part of graphene suspended and the other part supported by silica substrates.[95] When the same vertical bias was applied, Fermi levels of these two regions would be different due to the different dielectric materials: air and silica. Moreover, the silica substrate would help the supported part cool down quickly, leading to an enlarged temperature discrepancy with the suspended part. Benefitting from this design, 5−1000 times higher responsivity than other graphene photodetectors based on PTE effect was obtained under a laser of 476.5 nm. In contrast, in a subsequent report, Patil and co-workers studied graphene devices with fully suspended or silica-supporting graphene under a laser of 532 nm and concluded that both photoelectric and PTE existed in graphene

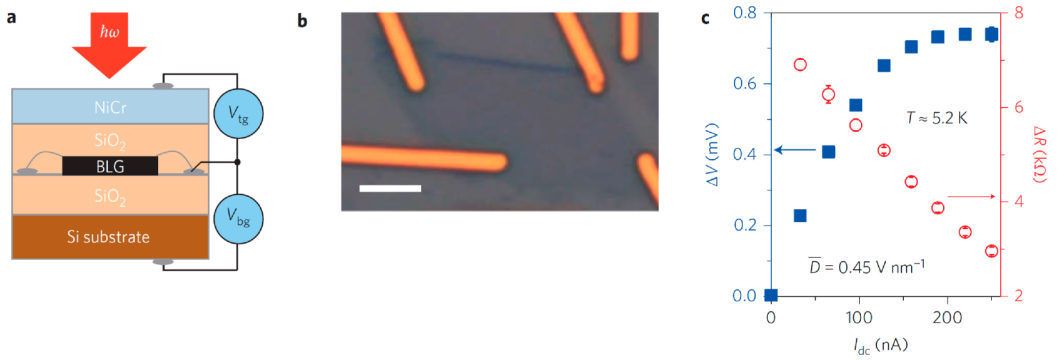

Figure 3. Bilayer graphene device and the typical optoelectronic response. (a) Schematic of device geometry and electric field-effect gating. (b) Optical micrograph of a bilayer graphene device. Scale bar, 5 mm. For clarity, the image shows the sample before top-gate dielectric and metal deposition. (c) Photoresponse of DGBLG. The sample is gated to a charge-neutral position with a displacement field of 0.45 V nm^{-1}. Blue squares are the photoresponse ΔV. Red circles are the electrical resistance change $\Delta R = \Delta V/I_{DC}$. Reproduced with permission from ref 99. Copyright 2012 Nature Publishing Group.

with a reciprocal relationship.[96] PTE played a major role when substrate existed but a minor role without substrate. Their contradictory results may derive from whether there is a junction with distinct Fermi levels in graphene. This issue is still controversial and needs to be addressed further.

Additionally, Stutzel *et al.* proposed another situation where PTE is the mainstream, the graphene nanoribbon phototransistors. Their device consisted of a graphene nanoribbon with a width of 10−35 nm bridging two metal electrodes on a SiO_2/Si substrate, and photocurrent was measured under a laser of 633 nm.[109] The key point of their devices is the restricted and reduced heat dissipation ability in graphene nanoribbons, which will enhance the importance of metal electrodes in the graphene cooling process under illumination and will lead to remarkable temperature difference (hundreds of times higher than graphene p−n junction) between graphene−metal and sole graphene area. Combined with large Seebeck coefficient difference between graphene nanoribbons and metal, this graphene nanoribbon phototransistor gave a photoresponse behavior fitting more PTE mode rather than photovoltaic mode without external bias. This report supplied another possibility to fabricate efficient graphene photodetectors based on PTE effect and to study the physical mechanism.

Beyond graphene, PTE effect in the photoresponse of the other two-dimensional materials such as metal dichalcogenides nanosheets has also been explored very recently. Buscema *et al.* studied the photoresponse of single-layer MoS_2 field-effect transistors by scanning photocurrent microscopy using sub-band-gap illumination.[72] They found that PTE effect was the dominant effect in the photocurrent generation in the single-layer MoS_2 transistors not only in sub-band-gap illumination (750 nm) but also in above-band-gap illumination (532 nm) where PV effect may also play a role. Importantly, a large-range-tunable Seebeck coefficient between -4×10^2 and -1×10^5 μV K^{-1} by the external gate electric field was observed in this device. The large Seebeck coefficient in single-layer MoS_2 may have a great potential in on-chip thermal power devices and harvesting the waste of thermal energy.

Photo-Bolometric Effect. Photoinduced bolometric effect is another mechanism proposed for the photoresponse of graphene photodetectors. This mechanism manifests as the dependence of conductivity on temperature. The unique heat properties of graphene, such as small electronic specific heat, electron−phonon decay bottleneck, and abundant hot carriers in graphene, support this mechanism firmly.[100,101] Yan *et al.* illustrated their study on this topic explicitly.[99] They used dual-gate bilayer graphene to fabricate an efficient hot electron bolometer. Through deliberate design, the uniformity of graphene was conserved and the graphene−metal junction was avoided as far as possible (Figure 3). The contribution of PV and PTE effects was excluded by the absence of output DC voltage signal under illumination. With a DC current input, the output DC voltage varied with the light on or off. The photoresponse, which was represented by ΔV, followed a different behavior mode from PC effect. They concluded that the photoresponse can be ascribed to bolometric effect occurring as electrons were heated. The response is given by

$$\Delta V = I_{DC}\Delta R = I_{DC}\frac{dR}{dT}\Delta T \quad (8)$$

where I_{DC} is the DC current applied; ΔT is the temperature change caused by light absorption, and R is the resistance.[99] Additionally, they clarified that at low temperature (<10 K) both optical and electrical heating were prominent, but when temperature was high (20−40 K), optical heating dominated. Lasers with various wavelengths from visible (658 nm) to near-infrared (10.6 μm) were used to test the photoresponse, implying broadband application of the device due to the unique energy band property of graphene.

In a subsequent report by the same group, the PV and bolometric effects were observed and discussed simultaneously in the device with similar structure under an infrared laser of 1560 nm.[101] They showed identical response time, which were used to testify that both effects originated from hot carriers. Unlike the bolometric effect mostly studied under low temperature of <100 K in aforementioned reports, Freitag *et al.* studied it at room temperature with a visible laser of 690 nm.[100] They used output DC (ΔI) current under certain bias instead of ΔV to characterize the photoresponse based on bolometric effect and defined the following bolometric coefficient to describe the gate-bias-dependent photoresponse behavior:

$$\beta(V_G) = \frac{\Delta I(V_G)}{\Delta T(V_G)} \quad (9)$$

They clearly distinguished the roles of PTE, PV, and bolometric effect in the photoresponses of single-layer graphene devices. They concluded that the latter two effects (PV and bolometric effects) were both driven by hot carriers and their contribution changed with the sweep of vertical gate bias. More particular works are necessary to study the bolometric effect, which is subtle and yet to be investigated thoroughly.

Deep insight into the various physical mechanisms of graphene photodetection is gained during the efforts toward making full use of the potential of graphene for high-performance photodetectors. Although graphene is very compatible with existing silicon-processing technologies, many improvements and modifications are required for its practical application. Inspired by the insightful understanding of physical mechanisms in graphene-based photodetection and by the excellent characteristics of two-dimensional atomic membranes, many methods have been developed to optimize the photoresponse of graphene and graphene-like 2D materials. The methodology mainly lies in state-of-the-art manipulation of device geometry and materials engineering.

Methodology: Device Geometry. Device geometry should be more pronounced in photonics and optoelectronics based on graphene and graphene-like 2D materials where only a two-dimensional, atomically thin sheet is applied as active photonic elements. Indeed, recent studies have demonstrated the great potential to modulate the photoresponse in graphene and graphene-like 2D materials by delicate device geometry designs which influence the photocarrier generation, transport, and light−matter interactions. In this part, we will discuss the dual-gate phototransistor, suspended photodetectors, photodetectors integrated with photonic structures of light−matter interaction enhancement, and some other novel designs in device geometry.

Dual-Gate Phototransistors. A phototransistor is a photoconductor gated with a third electrode. The additional vertical bias can be used to either open a band gap in bilayer graphene or control the Fermi level in graphene-based materials and thus change the conductive polarity and property. In terms of these functions, dual-gates can be used to realize junctions of areas with distinct Fermi levels or energy dispersion, which are essential for facilitating carrier transport and PTE effect.

In 2008, Ryzhii *et al.* developed a device model for dual-gate graphene nanoribbon (GNR) photodetectors for infrared and terahertz region light.[110,111] GNRs possess an advantage that its band gap is tunable by the width of ribbons,[112] which will be specified later. A universal back-gate voltage and a center-only top-gate voltage were combined to obtain an energy barrier between the center and the edge of graphene. When source-drain voltage was applied, potential difference would emerge and facilitate the photocarriers to transport and enhance the photocurrent (Figure 4).

On the basis of calculations, they developed a particular mode describing the relevance of photoresponse to ribbon width, source-drain voltage, light intensity, and frequency. Novel mechanisms were adopted to interpret the charge carrier transport process under different gate bias. At room temperature, the responsivity to the terahertz wave is expected to be up to 250 A/W under illumination of band-gap-matched wavelength and with source-drain bias of 5 V. Moreover, on the basis of the same structure, they obtained this value increased up to 800 A/W at a source-drain bias of 4 V with the graphene ribbon replaced by bilayer graphene.[113] Beyond the dual-gate idea, they develop a multiple-gate device geometry, which took advantage of one universal back gate and two parallel local top electrodes. Under appropriate bias conditions, this structure gave a p−i−n junction in multilayer graphene, which is different from aforementioned dual-gate induced n−p−n junction, although these two device geometries showed comparable responsivity.[25,114]

Dual-gate device geometry was also applied in graphene photodetectors harnessing PTE or bolometric effect, as demonstrated before.[91,92,97,99] It is worth noting that the responsivities of PTE devices are on the scale of 10^{-6}−10^{-4} A/W without external bias, which are largely inferior to those photoconductors. This is not hard to understand because the photocurrents are driven by external bias with a monotonic relationship in photoconductors. Neither the PV nor PTE effect is able to generate a built-in bias that is comparable with the external bias applied in those photoconductors. Thus, in graphene photoconductors, PC effect should be dominant and most attempts to improve their performance are launched on this principle.

Suspended Photodetectors. Suspended graphene shows excellent intrinsic electronic, thermionic, and other properties due to its well-conserved integrity and less exotic influences.[28] Substrates may affect the

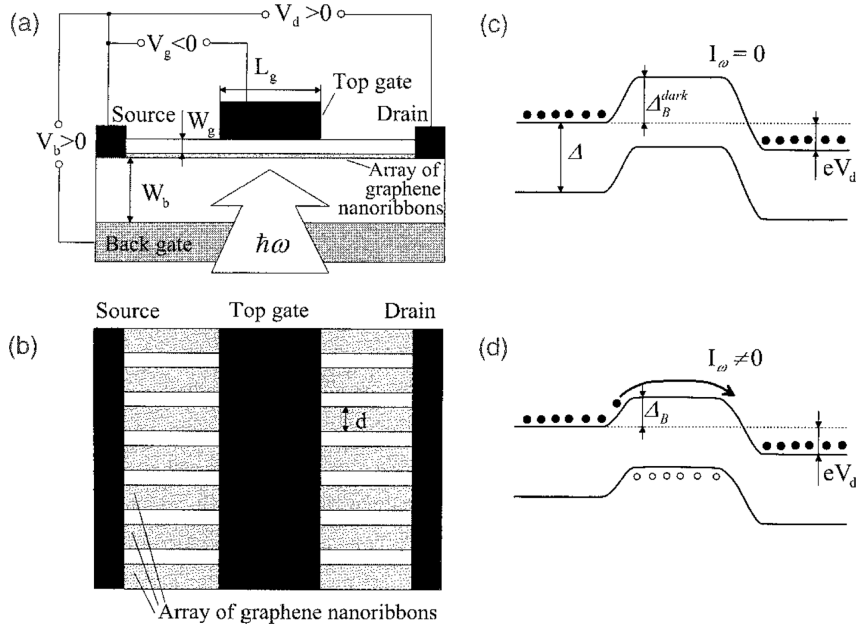

Figure 4. Schematic views of dual-gate GNR photodetectors: (a) side view, (b) top view, (3) device band diagrams under dark conditions, (d) under irradiation. Circles in (c) and (d) correspond to electrons and holes. Reproduced with permission from ref 110. Copyright 2008 The Japan Society of Applied Physics.

photocarrier behaviors in graphene and alter the photoresponse behavior in various ways from physical mechanism to photoresponsivity.[91,95,96] Therefore, much attention has been paid to suspended graphene for improved photodetection. Freitag *et al.* reported a center-suspended, side-supported graphene photodetector, which has been introduced in a previous section (Figure 5).[95] It worked based on PTE mechanism, and under illumination of 514.5 and 476.5 nm visible light and zero external bias condition, it presented much higher responsivity of $\sim 10^{-2}$ A/W compared with other PTE effect-based graphene photodetectors. The role of the suspension played in the remarkable performance improvement has yet to be studied.

Another suspended graphene photodetectors was reported by Vikram Patil and his co-workers.[96] They used complete suspended graphene to fabricate phototransistors and compared its performance with devices from silica supporting graphene. They concluded that the suspension of graphene made PC effect a dominant role instead of PTE effect, and the latter would rule the photoresponse when the substrate was presented. Even so, it is worth noting that, for all photocurrent measurements in this report, a 0.1 V source-drain bias was applied, which might induce unexpected enhancement of PC effect. After all, their devices gave a higher responsivity of ~0.4 A/W to visible light of 532 nm compared with its analogue.

Prechtel *et al.* described an ultrafast visible light (740 and 780 nm) response of suspended graphene grown by a liquid-based chemical vapor deposition (CVD) process, which is available at large scale and much easier to process than the mechanically exfoliated one. Time-resolved picosecond photocurrents of ~4 ps full width at half-maximum were observed in freely suspended graphene contacted by metal electrodes, which was attributed to the built-in electric fields at the graphene–metal interface. Moreover, PTE effect also plays a role in the device leading to a current with a decay time of ~130 ps.[89]

Photodetectors Integrated with Photonic Structures of Light–Matter Interaction Enhancement. One important limitation in improving responsivity of graphene photodetectors is the insufficient light absorption. To increase the graphene–light interaction path seems to be a feasible solution to this limit. This idea can be realized through integrating graphene to a structure which can confine light wave to a certain extent. There are three structures with the potential function to improve light–matter interactions in graphene: Fabry–Perot cavity, waveguide, and plasmonic structures. A Fabry–Perot cavity comprises two parallel reflecting mirrors, which can trap a photon with a selective wavelength between them for a long time. A waveguide is a one- or two-dimensional material in which a wave propagates and gets totally reflected on the wall. Thus, the wave will be restrained inside with small energy loss. Plasmonic structure is a kind of photonic structure where plasmon resonance happens. In this structure, incident light energy will be concentrated into a scale which is much smaller than wavelength, and the optical field will get enhanced largely, as well. Fabry–Perot cavity, waveguide, and plasmonic structures may enhance the photoresponse in graphene with different device geometries and physical mechanisms but with a similar device construction methodology by

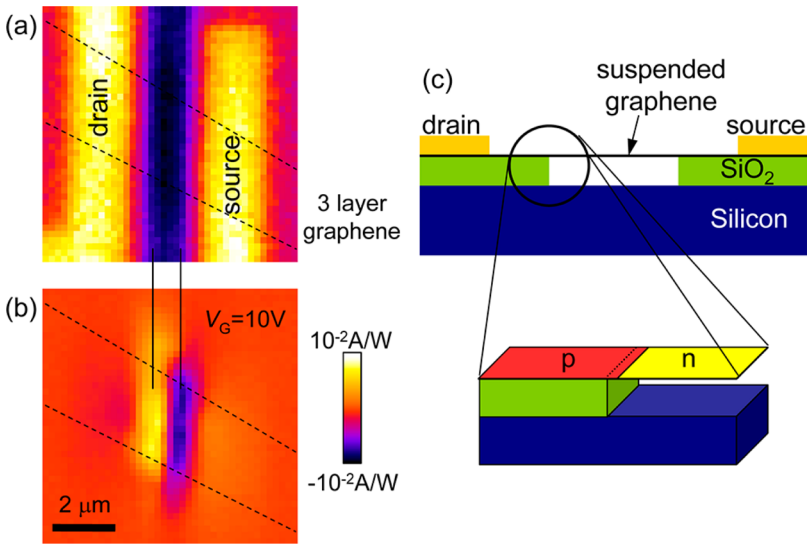

Figure 5. Partially suspended graphene p−n−p junctions. (a) Reflected laser light image of the device, showing the contacts, the SiO_2 support, and the trench. A three-layer graphene flake is exfoliated on top of the structure as indicated by dashed lines. (b) Spatially resolved responsivity of the graphene photodetector, measured with a wavelength λ = 514.5 nm and back-gate voltage V_G = 10 V. A peak responsivity on the order of 10^{-2} A/W is measured near the suspended-supported interface. (c) Schematic of the device, showing two 1 μm long supported graphene segments and the 1.5 μm long suspended part. The trench depth is 300 nm. The supported part is heavily p-doped by the substrate, while the suspended part is only lightly doped after annealing and can be switched to n-type or p-type by a gate voltage. The p−n junction is located about 100 nm inside the suspended part due to electrostatics. Reproduced from ref 95. Copyright 2013 American Chemical Society.

integrating graphene with other physical enhancement elements.

Ferreira *et al.* developed a mode for graphene-based photodetectors with two Fabry−Perot cavities.[49] They predicted absorption of ~100% by this device geometry at a given frequency. The operation wavelength λ of most efficient devices can be adjusted by the lengths of two cavities with them equal to $\lambda/2$ and $\lambda/4$, respectively. Moreover, Gan *et al.* found that graphene can reduce the reflection of the cavity by a factor of more than 100 as a return, making the graphene−light interactions larger than that in device geometry without a cavity.[52] Furchi and co-workers demonstrated a real graphene−cavity photodetector later, as shown in Figure 6a.[50] Their cavity was composed of two Bragg mirrors comprising alternating $AlAs/Al_{0.1}Ga_{0.9}As$ and SiO_2/Si_3N_4. Graphene was placed between these two mirrors. Light with a wavelength of ~850 nm can be trapped in this cavity and interact with graphene with a long path, resulting in light absorption of >60%. The photoresponsivity at this wavelength was enhanced remarkably compared with other wavelengths, demonstrating a value of 21 mA/W with an external bias of 2 V (Figure 6b). Similar enhancement effect has also been reported by Engel *et al.*[51]

The light absorption enhancement by graphene−waveguide integrations has been studied earlier.[44,45] Recently, Gan *et al.*, Pospischil *et al.*, and Wang *et al.* reported their respective photodetectors with similar device geometry as shown in Figure 6c almost in the mean time.[46−48] The wave propagating in the underneath Si waveguide was absorbed by graphene with dramatically elevated efficiency due to their coupling effects. Those authors investigated the graphene−wavelength interactions from different angles and demonstrated responsivities of ~0.1 A/W with an external bias of ~1 V under both 1550 and 2750 nm light. Impressively stable responses over broad light spectrum of 1310−1650 nm (Figure 6d) and operation rate up to 20 GHz were also demonstrated in these studies. Their studies elucidated the advantages of these kinds of devices including high-speed, broadband sensing, low-energy consumption, and compatibility with current technologies. They also pointed out that there is still large space for the devices to be optimized for higher performance in photoresponse.

The integration of graphene and plasmonic metal nanostructures has been explored to enhance the light−matter interaction in the reporty by Liu *et al.* using plasmonic gold nanoparticle arrays (Figure 6e).[41] The near-field oscillation and scattering effects in the gold nanoparticle arrays can trap light with selective wavelength (450−650 nm), depending on the size and shape of gold nanoparticles. With zero external bias, their photodetectors showed much higher intrinsic photoresponse than the same devices based on pure graphene without gold nanoparticles (Figure 6f). The maximum improvement of responsivity reached up to 1500% with a value of ~6.1 mA/W at 514 nm light. Echtermeyer *et al.* also observed the improvement of photoresponse in a similar structure with gold nanoparticles in the visible range (400−800 nm).[40] They focused mainly on the electric field enhancement of the junction of graphene−metal by plasmonic metal

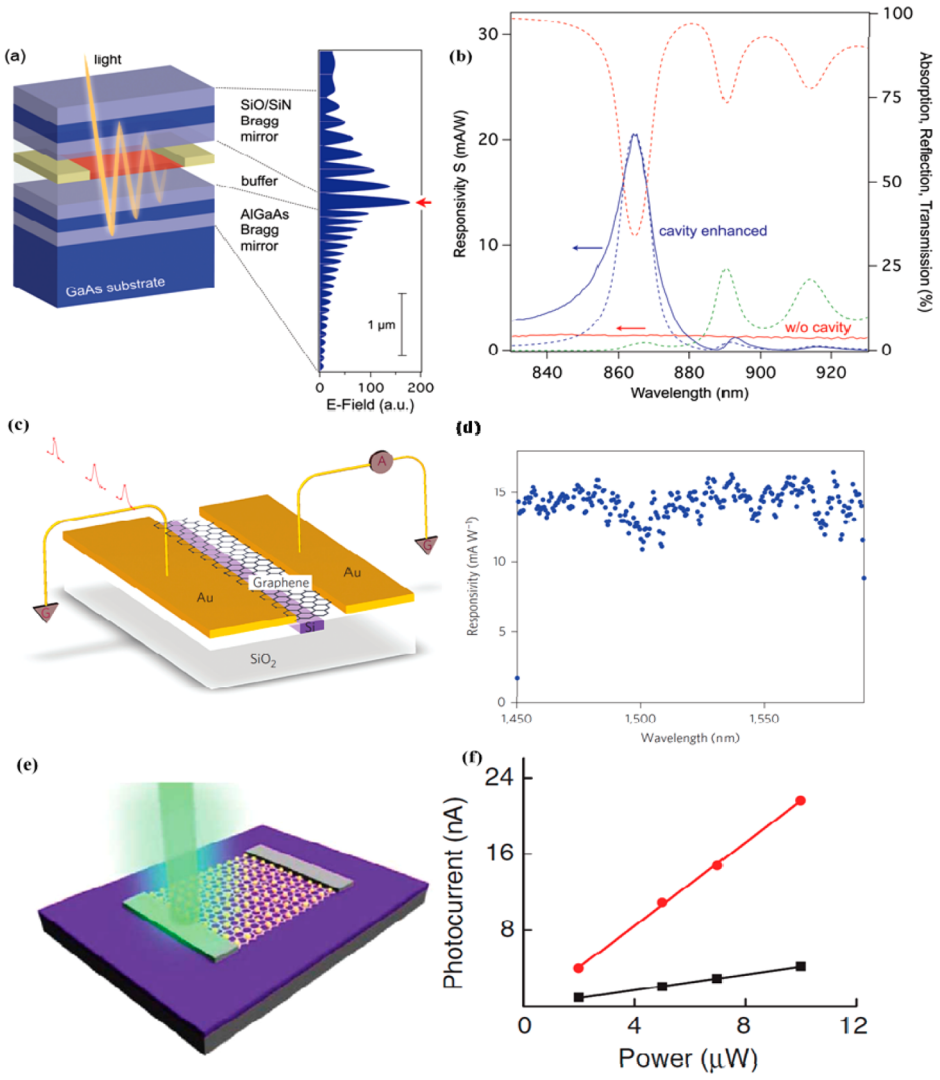

Figure 6. (a) Schematic drawing of a graphene microcavity photodetector. Distributed Bragg mirrors form a high-finesse optical cavity. The incident light is trapped in the cavity and passes multiple times through the graphene. The graphene sheet is shown in red, and the metal contacts are in yellow. (b) Spectral response of the bilayer graphene device with the structure in (a) with bias of 2 V. The dashed lines show reflection R (red), transmission T (green), and absorption A (blue). The solid lines are responsivity of bilayer with cavity (blue) and responsivity of bilayer without cavity (blue). A strong and spectrally narrow photoresponse is observed at the cavity resonance (855 nm wavelength). (c) Schematic of the graphene photodetector coupled with silicon bus waveguide. (d) Broadband uniform responsivity of device (c) over a wavelength range from 1450 to 1590 nm at zero bias. (e) Schematic of a graphene photodetector with Au particle plasmonic structure underneath. (f) Photocurrent generated as a function of laser power. The red and black lines indicate the response of a typical device with and without Au nanoparticles, respectively. Laser wavelength is 514 nm. Reproduced with permissions from refs 41, 46, and 50. (a,b) Copyright 2010 American Chemical Society. (c,d) Copyright 2013 Nature Publishing Group. (e,f) Copyright 2011 Nature Publishing Group.

structures and studied its dependence on light polarity and structural change in plasmonic elements. Moreover, Nie and co-workers fabricated another kind of device exploiting the plasmonic structures.[43] In their devices, the periodic ZnO nanorod array was placed vertically on a conductive plane which served as an electrode. The other side of the array was covered by single-layer graphene, onto which metal was deposited on the edge as the other electrode. The ZnO actually was the light harvester, and the nanorod array trapped light inside, thus enhancing the absorption by ZnO. The responsivity of 113 A/W was gained under illumination of 365 nm light with an external bias of 1 V. Interestingly, it was found that the rectifying feature of this junction can be changed by light. This device is worthy of deep investigations. As the plasmonic resonance only affects the close proximity of the structure, the extremely thin thickness of graphene can benefit from it more than other semiconductor materials. In another case, Shi *et al.* reported another plasmonic enhancement of photocurrent in graphene.[39] Two gold electrodes with sub-10 nm length spacing acted as optical antenna. Graphene was placed in this gap to form a photodetector. Plasmon-induced photocurrent enhancement from 2 to 100 was observed under light between 700 and 800 nm, with light

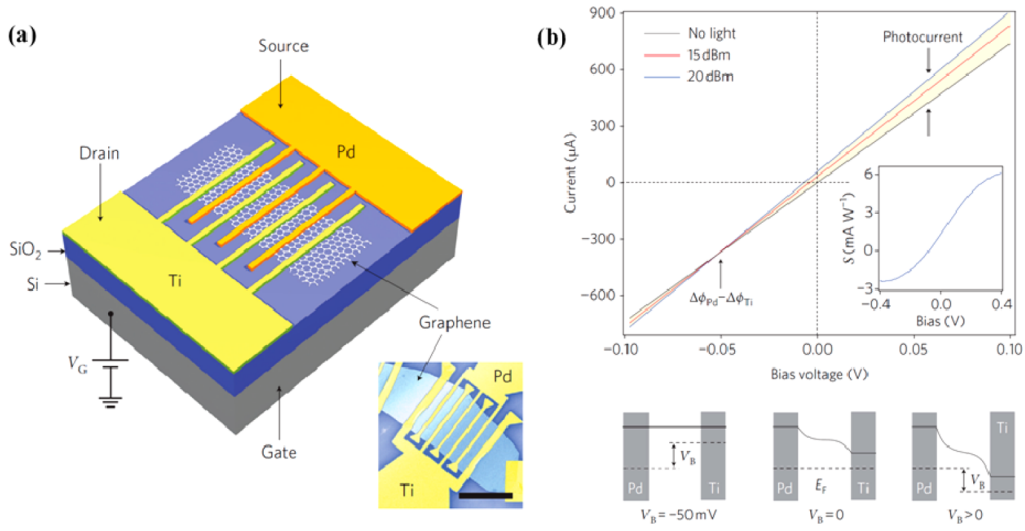

Figure 7. (a) Main panel: three-dimensional schematic of the photodetector. Bottom right: scanning electron micrograph of the photodetector. Scale bar: 5 mm. The spacing between the metal fingers is 1 mm, and the finger width is 250 nm. (b) Current *versus* source-drain bias (V_B) with and without light illumination, at an excitation wavelength of 1.55 mm. The difference between the colored (blue and red) and black lines (top in b) represents the photocurrent. Inset: measured external photoresponsivity of the photodetector as a function of the source-drain bias. The colored region denotes the magnitude of the photocurrent at an incident power of 20 dBm. The graphene band profiles (black lines, bottom in b) at V_B of 250 mV, 0, and positive bias, from left to right. V_B equals the difference in Fermi level between the palladium- and titanium-doped graphene. The dotted line represents the Fermi level. Reproduced with permission from ref 29. Copyright 2010 Nature Publishing Group.

polarity dependence reaching 99%. This device was far from understood as plasmon peak frequency, polarity dependence, and photocurrent enhancement changed from device to device.

Integrating graphene to photonic structures as mentioned above toward photodetectors possesses an apparent advantage: as the integrity of graphene is well-conserved, operation speed of this kind of device can be very high. Their performance can be improved with the progress in the manipulation of photonic structures and in the integration processing with graphene. We also note that integrating photonic structures with graphene-like 2D materials should have similar potential like that in graphene.

Other Designs in Device Geometry. The graphene–metal junction providing a built-in bias plays an important role in the photodetection process. Nevertheless, two identical metal electrodes locating two sides of the conductive channel form a symmetric and reverse electric field and snag the charge carriers' extraction. Mueller and co-workers reported their work on graphene photodetectors with asymmetric configuration by using titanium (Ti) and palladium (Pd) as two electrodes.[29] As the Fermi level of graphene (4.5 eV) is between the work functions of Ti (4.33 eV) and Pd (5.5 eV), an energy level alignment facilitating electron transport from Pd to Ti was formed (Figure 7). Consequently, this device benefited from both PC and PV effects and gave a responsivity of 6.1 mA/W with a source-drain bias of 0.4 V under illumination of 1.55 μm light. This device was deployed in a 10 Gbit s^{-1} optical data link for error-free detection of the optical bit stream, showing a fast response speed. Hsieh *et al.* reported a so-called "optothermal" graphene photodetector.[93] Graphene was deposited on the surface of polarized lead zirconate titanate (PZT) substrates. The polarization of PZT was used to replace vertical gate bias to accumulate carriers in graphene sheets and to control the conductivity of graphene. The polarization of PZT can be changed by temperature, which was changed by infrared illumination. The final output was the conductivity change in graphene. It is apparent that this process has nothing to do with the thermal or optical properties (except the transparency) of graphene, which only serves as a conductor. Variable operation wavelength is also possible for this kind of device as only the piezoelectric effect of PZT is essential. Even so, this device is a good exploration for low-energy consumption devices and is highly implantable to other materials and 2D materials.

Kang *et al.* used a layer of Al_2O_3 to passivate the surface of graphene in a photodetector.[115] They found that the polarity of photocurrent under ultraviolet illumination of 385 nm reversed before and after this passivation. This switch was attributed to the different doping states of graphene in ambient and passivated environment, and the graphene–metal junction was believed to be responsible for the photoresponse process. They did not give the exact photoresponsivity, but it should be in the scale of 10^5 A/W with an external bias of 0.1 V upon our estimation, which is a very high value for pure graphene devices. They also announced a carrier lifetime of 0.5 ps, which is small enough for fast device operation speed. Their device is very promising for both fundamental studies in pure graphene photoresponse and practical applications in photonic and optoelectronic devices.

Comb-shaped metal contacts were designed to increase the contact area of CVD monolayer MoS_2 with electrodes in a phototransistor by Zhang *et al.*[79] Due to the large area growth of CVD MoS_2, this strategy can be easily adopted to fabricate large area devices up to millimeter size with tens of comb-shaped metal contacts. This comb-shaped metal contact was believed to enhance the photocarrier generation, and the photoresponses were indeed enhanced with a responsivity of 2200 A/W under illumination of 532 nm with an external bias of 1 V, much larger than single source-drain metal contact devices.

Methodology: Materials Engineering. Another way to modulate the photoresponse in two-dimensional materials is materials engineering. Through controllable materials engineering, the intrinsic electronic and optical properties in graphene and graphene-like 2D materials can be regulated, or the main disadvantages for limiting the photoresponses can be compensated. We will first discuss briefly the graphene-based photodetection from three strategies, including shaped graphene, chemically doped graphene and reduced graphene oxide, and hybrids and heterostructures based on graphene. Then the emerging photodetection from graphene-like 2D materials will be discussed with the most recent progress.

Shaped Graphene. The properties of graphene get reshaped when it is scaled to nanostructures such as nanoribbons. GNRs possess width-dependent band gap due to the breaking of the atomic symmetry, which is absent in pristine graphene sheets.[112,116,117] The emergence of band gap may induce enhanced separation of photon-induced excitons, higher carrier extraction efficiency, and more selective responses to light wavelength, as well. Moreover, GNRs show reduced heat transport capability, which can be exerted in PTE photodetectors.[118] Ryzhii proposed the device mode of long wavelength dual-gate photodetectors based on GNR.[110,111] They demonstrated diverse working modes of GNR photodetectors with different graphene−metal junction types and vertical gate bias. Under illumination of band-gap-matched wavelength and with source-drain bias of 5 V, they predicted high photoresponsivity of ~250 A/W with a GNR with band gap of 50 meV corresponding to a width of ~20 nm. Chitara *et al.* demonstrated their real photoconductors based on GNRs with a width of ~5 nm.[119] They analyzed their device performance through PC effect and gave a responsivity of ~1 A/W with incident wavelength of 1550 nm and external bias of 2 V. This suppressed responsivity, compared with the value predicted in previous reports, may be ascribed to the large band gap, lack of gate bias, and mismatch between incident wavelength and band gap. The reshaped thermal property of GNR has also been applied in photodetection. Stutzel *et al.* fabricated phototransistors based on GNR and studied its zero external bias photoresponse.[109] They tested the photocurrent of devices under a laser of 633 nm and paid more attention to the internal mechanism which was proven to be PTE effect. The reduced heat transport capability of GNR and dramatic Seebeck coefficient differences between graphene and metal were believed to be responsible for the dominance of PTE effects in their devices. The optical properties of GNR can be further enhanced by periodic structures due to plasmonic effects. Freitag *et al.* fabricated the photoconductors based on GNR arrays with width below incident wavelength, as shown in Figure 8a.[120] When infrared or terahertz wave with polarization perpendicular to the GNR axis falls on this structure, the photons would interact with the hybrid plasmon−phonon quasiparticles and form plasmonic photocurrent in addition to the conventional photon-induced electron−hole photocurrent. Under this regime, periodic GNR structure gave a 6 times higher photoconductivity than pristine graphene of the same overall dimension, as shown in Figure 8b. Moreover, this photoresponse was proven to be dependent on and thus tunable by vertical gate bias and ribbon width.

Zhang *et al.* reported another architecture of graphene, which is continuous graphene quantum dots (GQD), as shown in Figure 8c.[121] The small GQD size down to ~7.5 nm would create a band gap due to quantum confinement effect, and meanwhile, the edge of these GQDs would introduce midgap state bands which act as electron-trapping centers. The emerging ample energy states enhanced the photoresponse of graphene film and gave a responsivity of ~8.61 A/W under light of 532 nm with external bias of 0.1 V. This value is 3 orders of magnitude higher than the device reported based on pristine graphene. The space to enhance photodetection performance of graphene-based materials through architecture design is far from exhausted, especially due to the recent rising research on graphene plasmonics.[53] Much progress can be expected to emerge in the future. We note that shaped graphene-like 2D materials such as shaped MoS_2 nanosheets may also have a high potential in the modulation of their photoresponses, although little work has been done in this direction.

Chemically Doped Graphene and Reduced Graphene Oxide. Chemical doping in graphene is an effective method to introduce energy states into graphene and break the symmetry of two-dimensional atomic structures. Thus, chemical doping and reduced graphene oxide, which essentially is one kind of doping with oxygen or hydroxyl as dopants, support great potential in modifying electronic, optical, and thermal properties of graphene.[30,122−124] Yan *et al.* demonstrated that heavily doped graphene by $(C_2H_5)_3OSbCl_6$ possessed an impressive absorption in the infrared region up to 40%.[124] Chang *et al.* and Shen *et al.* systematically studied the evolution of band gap as well as optical properties of reduced graphene oxide (RGO) with different reduction levels, revealing a tunable band

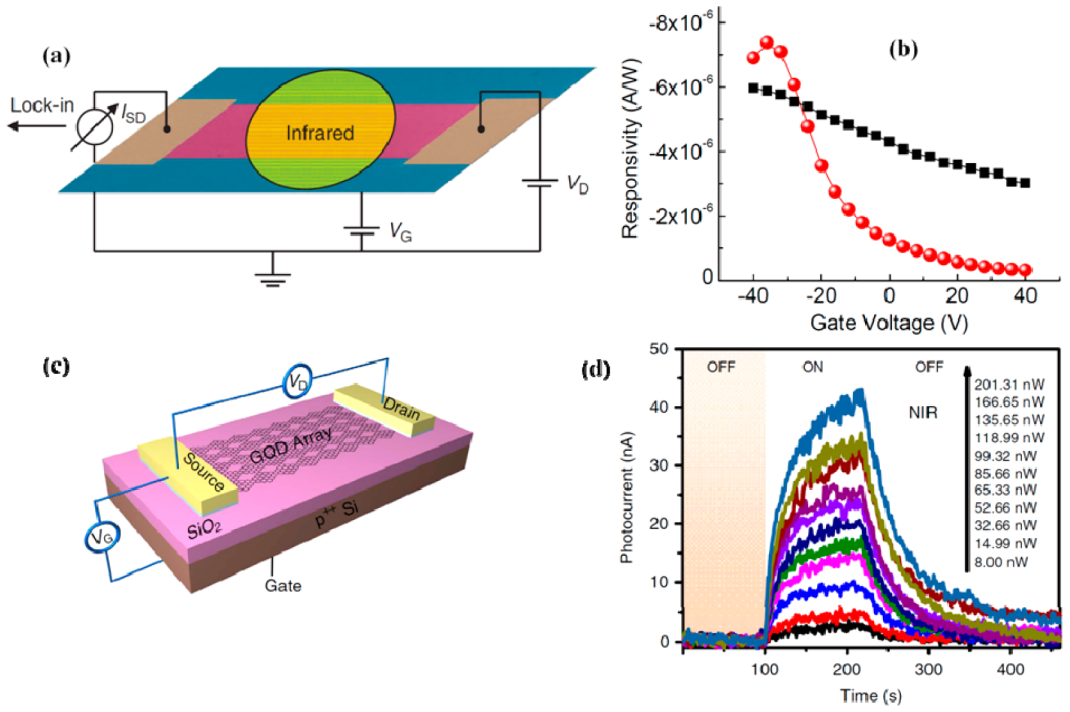

Figure 8. (a) Schematic of the photoconductor and measurement setup. Infrared laser light at 10.6 mm is chopped at 1.1 kHz, and the photocurrent is analyzed by a lock-in amplifier referenced to the chopping frequency. (b) Photoconductance G ($G = I_{ph}/V_{bias}$, I_{ph} is photocurrent, V_{bias} is the applied bias on this photoconductor) of 140 nm GNR superlattice (red spheres) and 2D graphene (black squares) upon photoexcitation with the same laser power $P = 66$ mW and applied bias of -2 V. (c) Schematic of a phototransistor based on GQD structure. (d) Time-dependent photocurrent measurements of device in (c) under illumination of 532 nm with variable intensity. Gate bias is 0 V. Source-drain bias is 20 mV. Reproduced with permission from refs 120 and 121. Copyright 2013 Nature Publishing Group.

gap from 0.02 to 2.2 eV for RGO.[35,36] Peters and co-workers fabricated a photodetector based on graphene which is half n-doped by poly(ethylenimine) and the other half p-doped by oxygen in ambient. The p−n junction formed accommodated a PV effect underlying the device photoresponse to visible light (476, 514, and 633 nm).[87]

Nevertheless, the RGO seems to be more favorable for the application in photodetectors, which may be attributed to its easy processing and solution-processable characters. Chang and co-workers reported ultraviolet (UV), visible, and near-infrared (NIR) response of photodetectors based on few-layer reduced graphene oxide (FRGO) in two successive works.[34,35] The band gap of the RGO can be tuned from ~2.2 to ~0.5 eV by facile annealing treatment at 150 °C from 90 to 260 min. The best device demonstrated responsivity of ~0.86 A/W to UV (370 nm) with external bias of 10 V and ~0.7 A/W to NIR (895 nm) with external bias of 19 V, respectively. Moreover, through first-principle calculation, they delved deeply and found that oxygenous defects which acted as the electron traps could significantly influence and therefore regulate the photoresponses (Figure 9). These traps would also drag the response speed and make photocurrent slow in both generation and decay. These effects appeared all across the wavelength from UV to NIR. Annealing treatment could not only adjust band gap of RGO but also control the trap quantity by reducing oxygenous defects. More importantly, the atomic structure evolution and oxygenous defects could be well-controlled to realize the external quantum efficiency for NIR up to ~97% in FRGO, which is the highest from pure graphene to graphene-based derivatives.

Besides, another two works on photoconductors based on RGO have been reported by Chitara *et al.*[119,125] They used hydrazine to reduce graphene oxide in solution and tested their response to NIR (1550 nm) and UV (360 nm) illumination under a bias of 2 and 1 V, respectively. Responsivities of 0.04 and 0.12 A/W were separately obtained for NIR and UV. PC effect was used to explain the photoresponse, and PTE effect was ruled out. With the traps, the crack and defect in graphene can induce trap states used to improve the photon-induced exciton dissociation in graphene. Kurra *et al.* used few-layer graphene and graphite to fabricate photoconductors and measured their response to NIR light.[126] The photoresponse behaviors of those two kinds of devices showed reverse polarity and distinctly manifested two different underlying mechanisms, which are PC and PTE effect, respectively. In particular in this report, due to the rigorous synthesis of graphene and ambient environment where measurement was carried out, the apparent photoresponse of few-layer graphene should possess an internal link to the defect in graphene

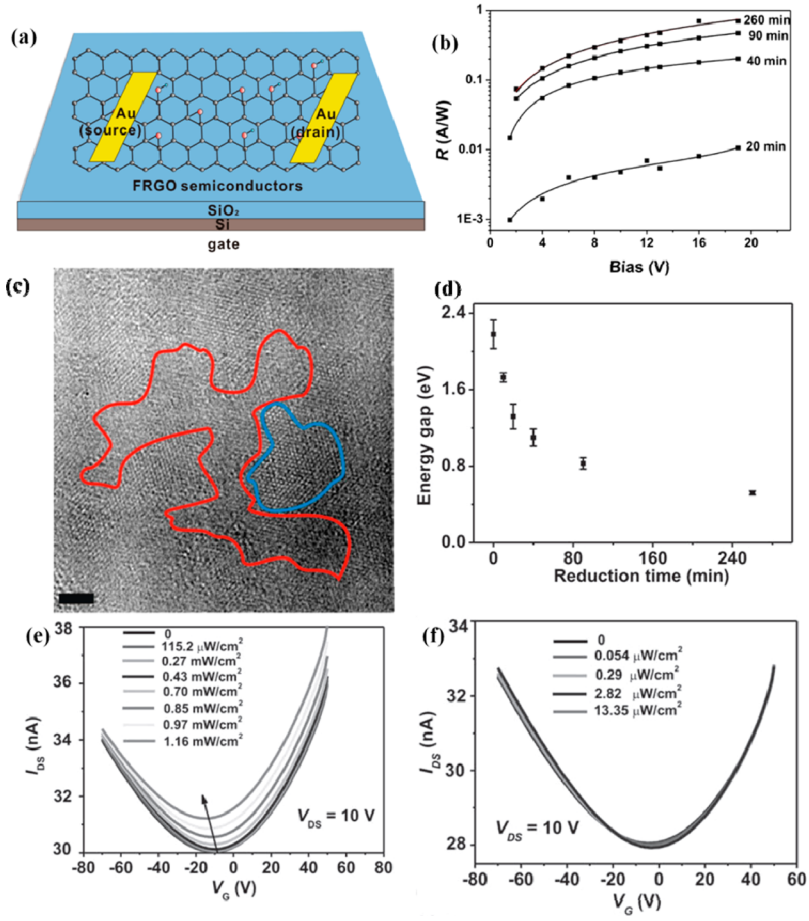

Figure 9. (a) Scheme for a FRGO phototransistor. (b) Responsivity *versus* bias for FRGO/SiO_2/Si-based rigid infrared phototransistor devices based on FRGO with different reduction times (20, 40, 90, 260 min). Incident radiation wavelength is 895 nm; power is 14 mW/cm^2. Black lines in (a) are fitted curves, V_G = 0 V. (c) TEM image showing atomic structure of graphene oxide. Red line defines an area of highly disordered structure, and blue line defines an area of relatively ordered structure. (d) Calculated energy band gap of FRGO *versus* reduction time. (e) $I_{DS}-V_G$ curves of 90 min FRGO phototransistors under radiation at 370 nm and (f) 470 nm. Reproduced with permission from refs 34 and 35. (a–c) Copyright 2013 American Chemical Society. (d-f) Copyright 2010 Wiley-VCH Verlag GmbH & Co. KGaA.

structure and oxygen adsorbed on graphene surfaces evidenced by the high D peak in the Raman spectrum.

Hybrids and Heterostructures Based on Graphene. Considering the excellent carrier transport property of graphene and the abundant organic or inorganic optical materials, it is reasonable to have the idea to combine them together and spare the light-harvesting burden from graphene to other materials with better and selective optical properties. Compared with elaborative designs in device geometry or precise lithography in graphene shape, hybridization and heterostructures are rather facile methods to realize graphene photodetectors with high responsivities.

The ways to obtain hybrids based on graphene are diversified, from chemical growth to physical deposition, even simple spin-coating and drop-casting the additive component on graphene sheets. The appearance of the exotic components not only supplies an efficient light harvester in a photodetector but also creates interfaces in the hybrid systems which can enhance the separation of photon-induced excitons. For instance, lead sulfide quantum dots (PbS QDs) are a kind of promising light-harvesting material for its size-dependent band gap. A series of photodetectors using graphene sheets decorated by PbS QDs as active layers have been reported.[23,60,61,70] As a representative, Sun *et al.* fabricated a NIR phototransistor based on graphene–PbS QDs hybrid film, with pyridine-capping PbS QDs drop-casted on CVD-grown monolayer graphene from colloid solution (Figure 10).[23] With the high light-harvesting capability of PbS QDs and well-conserved carrier mobility in graphene, this device showed responsivity as high as $\sim 10^7$ A/W at low light intensity of 895 nm NIR radiations with external bias of 5 V. By studying the time-resolved photocurrent, the photoresponse dynamics was clarified. The energy level alignment of PbS QDs and graphene was proven to be important for the exciton separation and carrier transfer in the QD–graphene interfaces. Both photon-induced holes and electrons were able to transfer into graphene but with different speed. Net electrons staying in the PbS QD layer formed an additional vertical

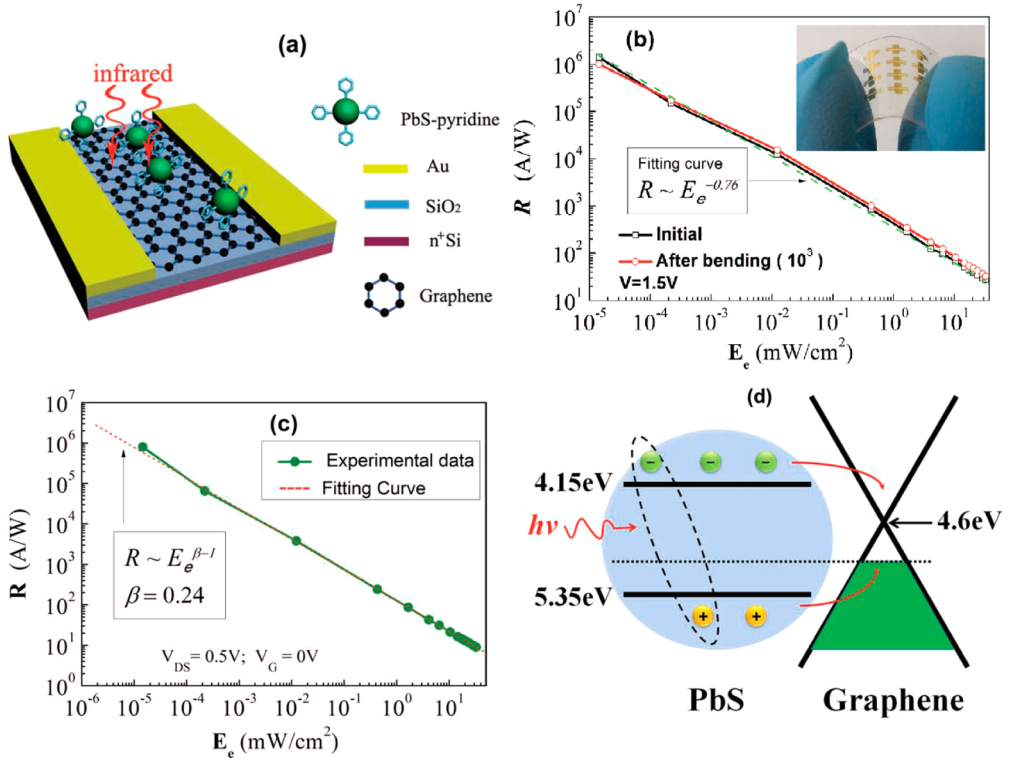

Figure 10. (a) Schematic diagram of a graphene photoconductor modified with PbS QDs under light illumination. (b) Responsivity as function of light irradiation when this photoconductor is fabricated on a PET plastic substrate. Measurement was carried out both before and after bending the device with radium of 7 mm for 1000 times. Inset: real image of device. (c) Responsivity of a photoconductor on a SiO_2/Si substrate as functions of light irradiation. (d) Schematic diagram for charge generation at a PbS QD/graphene heterojunction under light illumination. Reproduced with permission from ref 23. Copyright 2012 Wiley-VCH Verlag GmbH & Co. KGaA.

bias which led to photoresponse of graphene. The photoresponse behavior was tunable through vertical gate bias. Moreover, this device gave stable photoresponse on the PET plastic substrate after 1000 times bending test, demonstrating its flexibility. Similar NIR photodetectors with mechanically exfoliated graphene and spin-coated PbS QDs have been reported by Konstantatos and co-workers, giving even higher responsivity.[61] In another case, graphene-on-MoS_2 binary heterostructures were explored as a photodetector and demonstrated ultrahigh photosensitivity of 5×10^8 A/W at room temperature and 1×10^{10} A/W at 130 K under illumination of 635 nm with external bias of 0.1 V.[71] The graphene-on-MoS_2 heterostructures also had gate-tunable persistent photoconductivity because of gate-tunable charge exchange between the graphene and MoS_2 layers and may be applied as a rewritable optoelectronic switch or memory.

Another form of hybridization happened to RGO, with either simple mixture or *in situ* growth of additives. Although RGO is not comparable with pristine graphene on carrier transport capability, it possesses the advantage of solution processability. Chang and co-workers demonstrated the studies on *in situ* growth of nanocrystals on RGO in successive reports.[58,59] In their first work, RGO was functionalized by pyrenebutyrate to form the growth center of nanocrystals. Then precursors were added to grow cadmium sulfide quantum dots (CdS QDs). Finally, obtained CdS QD−RGO hybrid films can be used to sense UV and visible light and applied as optoelectronic switches with high on−off ratios. In the latter work, they functionalized RGO by mixing ZnO QDs instead of organic molecules. Then, based on ZnO QDs on RGO, ZnO nanorods were grown *in situ* as heterostructures. Using the ZnO nanorod−RGO hybrids, they fabricated visible−blind UV photodetectors with better performance than ZnO QD−RGO hybrids and pure graphene, giving responsivity of ~22.7 A/W under 370 nm illuminations and external bias of 20 V. Similar graphene hybrids were also developed by Cao *et al.* using CdS QDs and Geng *et al.* using CdSe QDs.[54,56]

There are many possibilities to realize graphene-based hybrids for photodetectors. A variety of attempts have been done and reported, as listed in Table 1. It is worth noting that, although hybridization is an effective pathway to high-performance and selective photodetectors based on graphene, it suffers from low operation speed due to the long carrier transfer and trap times. This kind of device may be more suitable for application demanding more in responsivity rather than response speed such as remote sensing of light or gas sensors where speed is not the major concern.

Photodetection Based on Graphene-like 2D Materials. Recently, there is a growing interest in photodetection

TABLE 1. Summary of Reported Photodetectors Using Hybrids and Heterostructures Based on Graphene

graphene materials	hybridized component	operation wavelength	responsivity, R (A/W)	external bias (V)	remarks (D, t, *etc.*)	ref
GO	$Ti_{0.91}O_2$	white light	—	—	EQE = ~1.5%	55
RGO	CdSe QDs	473 nm	—	2	photoconductivity = $\sim 10^2$ S/m	56
SLG[a]	O_2	350−700 nm	—	0.1	—	57
RGO	TiO_2	300−800 nm	—	5	$D = 2.3 \times 10^{12}$ Jones $t = 0.1$ s	21
RGO	CdS QDs	white light	—	—	EQE = ~1.2%	59
SLG	TiO_2 thin film	254 nm	—	0.2	$t = 130$ s (95%)[d]	22
SLG	PbS QDs	white light	$\sim 2.8 \times 10^3$	0.001	—	60
SLG, BLG[b]	PbS QDs	532 nm, 1050 nm, 1600 nm	$\sim 5 \times 10^7$	5	$D = 7 \times 10^{12}$ Jones $t > 0.01$ s (532 nm)	61
SLG	PbS QDs	895 nm	$\sim 10^7$	5	$t = 0.26$ s (80%)[d]	23
SLG	PbS QDs	442 nm	—	0.0001	—	70
SLG	chlorophyll	683 nm	$\sim 10^6$	1	$t = 0.11$ s	65
SLG	n^+ silicon	400−900 nm	0.435	—	$D = 7.69 \times 10^9$ Jones $t = 0.04$ s	64
SLG	monolayer MoS_2	650 nm	$\sim 10^7$	1	$t > 50$ s	68
SLG	few-layer MoS_2	635 nm	10^{10} at 130 K 5×10^8 at RT[c]	0.1	—	71
SLG	few-layer MoS_2	white light	—	0.1	—	67
SLG	ZnO QDs	325 nm, 445 nm	$\sim 10^4$	0.001	$t = 5$ s	69
SLG	ZnO QDs	365 nm	—	3	$t = 2$ s	63
RGO	ZnO nanorods	370 nm	~22.7	20	—	58
SLG	graphite QDs	325 nm	$\sim 4 \times 10^7$	1	—	66
SLG	C_{60}	white light	—	0.01	—	62

[a] SLG: single-layer graphene. [b] BLG: bilayer graphene. [c] RT: room temperature. [d] Percentage of photocurrent change used to define response time.

and photodetectors based on graphene-like 2D materials, especially layered metal chalcogenides such as MoS_2, GaS, GaSe, GaTe, WS_2, and their hybrids or nanocomposites.[73−80,127,128] Although graphene-like 2D materials and graphene are very different from the composition and properties, they all inherit the two-dimensional quantum limit which significantly influences the electronic transport and photoresponse.[1,11,73−80] Unlike zero gap graphene, some layered metal chalcogenides are semiconductors with direct or indirect band gaps and can have a mobility of as high as 200 cm^2/Vs with an on−off ratio of about 10^8, showing a great potential for optoelectronic applications.[11] Both photoelectric and photo-thermoelectric effects have been found to play roles in the photoresponses of layered metal chalcogenide nanosheets (see more discussions in the physical mechanisms part), and more work needs to be done to clarify the physical mechanisms of photodetection in different graphene-like 2D materials and device geometry.[72,73,77,80] By carefully choosing graphene-like 2D materials and controlling the thickness, the photoresponse can be optimized in the responsivity and response speed.

The innate band gaps of some graphene-like 2D materials, on the other hand, bring selective photoresponse compared with the broadband response of graphene. This feature may be an advantage in some particular applications. Yin *et al.* reported their phototransistors based on mechanically exfoliated single-layer MoS_2.[73] The phototransistors were almost blind to light with a wavelength >673 nm, which corresponds to the band gap of single-layer MoS_2 (~1.83 eV). They showed a photocurrent generation solely dependent on radiation power and could reach a photoresponsivity of about 0.42 mA/W at 1 V drain voltage and 7.5 mA/W at a gate voltage of 50 V under the illumination of 550 nm (Figure 11a,b). The phototransistor also showed good stability in cycling performance and had a response speed of about 50 ms. Similar phototransistors sensing from UV to NIR (900 nm) can be built using mechanically exfoliated multilayer MoS_2 with a photoresponsivity of about 100 mA/W, as shown by Choi *et al.*[74] Their performance can be further enhanced by improving the mobility of MoS_2, the contact quality, and positioning techniques, leading to photoresponse in the 400−680 nm range and a photoresponsivity of about 880 A/W at a wavelength of 561 nm and a long response time of 4 s.[77] Zhang *et al.* prepared phototransistors based on CVD-grown large area single-layer MoS_2.[79] Their photoresponses were significantly influenced by charged impurities at the MoS_2/substrate interfaces and adsorbents from ambient air. The time-resolved photoresponses were also dependent on temperature with fast switch on−off speed at low temperature. Their CVD MoS_2 phototransistors demonstrated a high photoresponsivity of 2200 A/W under illumination of 532 nm. Lee reported a phototransistor with a variable optical band gap dependent on thickness.[75] A single-layer MoS_2 had a band gap of ~1.83 eV, while the energy gap decreased to ~1.65 and 1.35 eV for bilayer and trilayer MoS_2, respectively. As a result, single-layer and bilayer MoS_2 were more proper for green light detection, and trilayer showed good performance in red light detection. Similar photodetection was also demonstrated using multilayer WS_2 by Perea-López *et al.*[81] In their report, the responses of photodetectors were highly dependent on radiation energy for light

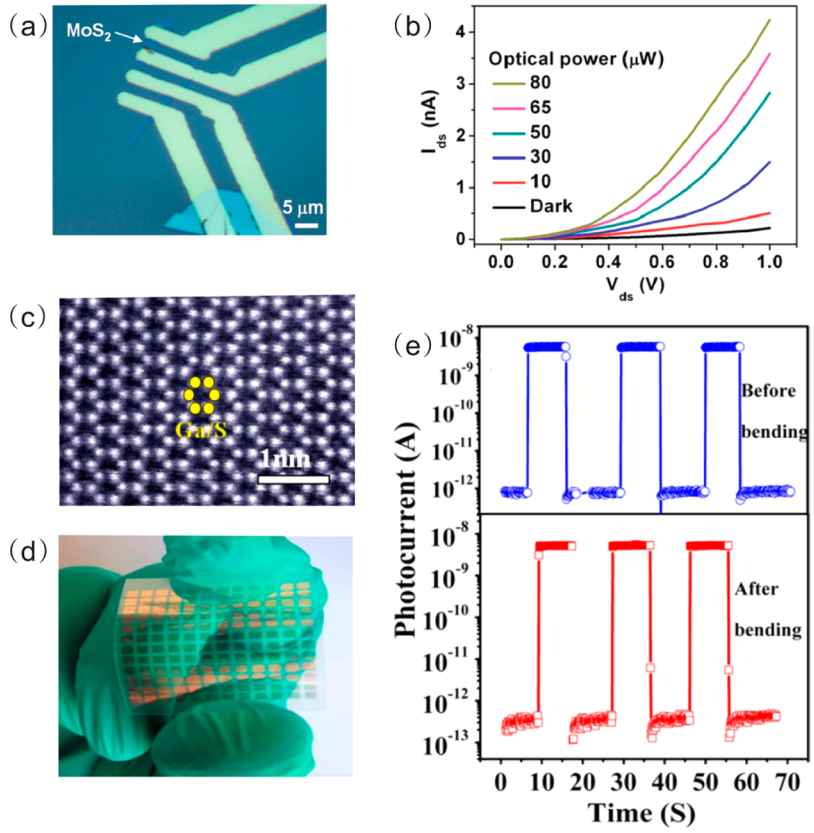

Figure 11. Phototransistors and photodetectors based on two-dimensional metal chalcogenide nanosheets. (a) Optical image of a MoS_2 phototransistor. (b) Photoresponse of MoS_2 phototransistor. (c) Atomic image of GaS nanosheets. (d) Flexible GaS photodetector devices. (e) Photoresponses of flexible GaS photodetector. Reproduced and adapted from refs 73 and 78. Copyright (a,b) 2012 and (c–e) 2013 American Chemical Society.

ranging between 457 and 647 nm with a responsivity of 92 μA/W and response time of about 5 ms.

Besides MoS_2 and WS_2, other layered metal chalcogenides like Ga-based chalcogenides including GaS, GaSe, and GaTe have been investigated for photodetection applications, as well. Hu *et al.* fabricated highly sensitive photodetectors based on GaS nanosheets (Figure 11c–e).[78] The reported photodetectors fabricated on polyethylene terephthalate (PET) substrates were sensitive from UV to visible light with a photoresponsivity of 0.95 A/W for 550 nm, 1.56 A/W for 490 nm, 15.3 A/W for 365 nm, and 19.2 A/W for 254 nm light. The photosensitivity linearity (in dB) or linear dynamic range (LDR, given by $LDR = 20 \log(I_{ph}/I_{dark})$ where I_{ph} is the photocurrent at 1 mW cm^{-2} radiation) of the devices reached 97.7 and 78.73 dB for devices on SiO_2/Si and PET, respectively. Importantly, 20 bending cycles showed no harm to the performance of flexible photodetectors on PET, and the response time was acceptable at the level of 30 ms. Similar photodetectors were built using few-layer GaSe nanosheets to replace GaS nanosheets.[76,82] The maximum responsivity of GaSe nanosheets reached 2.8 A/W, and a high external quantum efficiency of 1367% was achieved at 254 nm. Liu *et al.* reported a novel photodetector based on another kind of layered Ga-based chalcogenides, GaTe nanosheets.[80] The GaTe nanosheets had a mobility of 0.2 $cm^2\ V^{-1}\ s^{-1}$, and the resulting photodetectors were proven to be very sensitive to visible light at 532 nm with a responsivity of 10^4 A/W, much higher than other metal chalcogenide photodetectors. The response time was at the acceptable level of 6 ms.

The performance of some most promising photodetectors based on graphene or graphene-like 2D materials are listed in Table 2. Pure graphene-based photodetectors have the fastest response speed but very low responsivity, while graphene hybrids have highest responsivity but much lower response speed. Pure graphene-like 2D materials have very different responses highly dependent on the type of 2D materials with the best performance having slightly higher response speed but much lower responsivity than graphene hybrids. It is worth noting that the operation wavelengths specified in this article are the testing wavelength used for either specific or maximum photoresponse. Theoretically, the devices based on graphene-like 2D materials and the devices with graphene as conducting materials should be able to respond to shorter wavelength. Graphene devices with zero band gap graphene as light sensitizer may be able to work under both longer and shorter wavelengths.

TABLE 2. Representative Photodetectors Based on Graphene or Graphene-like 2D Materials in Terms of Methodology

methodology	materials	mechanism	operation wavelength	responsivity (A/W)	external bias (V)	remarks (*D*, *t*, *etc.*)	ref
dual-gate	BLG	PV, PC	terahertz and infrared	800	4	$D = 4 \times 10^{12}$ Jones	113
	BLG	PTE	480—750 nm	~0.0015	0	—	97
	BLG	photo-bolometric	658—10600 nm	—	—	$t < 1 \times 10^{-9}$ s, ($T < 40$ K)	99
suspended	TLG[a]	PTE	476.5 nm, 514.5 nm	~0.01	0	—	95
	SLG (microribbons)	PC, PTE	532 nm	~0.4	0.1	—	96
integrated with photonic structures	BLG (microcavity)	PC	830—900 nm	0.021	2	—	50
	BLG (waveguide)	PC, PV	1450—1590 nm	0.108	1	—	46
	SLG (plasmonic array)	PV	400—700 nm	0.0061	0	—	41
shaped	GNR	PC	1550 nm	~1	2	$t > 160$ s	119
	GQD	PC	532 nm	8.61	0.1	$t > 100$ s	121
	SL-MoS_2 (comb-shaped)	PC, PV	473, 532 nm	2200	1	$t = 500$ s (RT), 0.055 s (<153 K)	79
chemically doped	RGO	PC	370—895 nm	0.86 (370 nm) 0.7 (895 nm)	10 (370 nm) 19 (895 nm)	$t = 20$—52 s	34,35
hybrid and heterostructure	SLG, BLG (PbS QDs)	PC	532 nm, 1050 nm, 1600 nm	$\sim 5 \times 10^7$	5	$D = 7 \times 10^{13}$ Jones, $t > 0.01$ s (532 nm)	61
	SLG (few-layer MoS_2)	PC	635 nm	10^{10} at 130 K 5×10^8 at RT	0.1	—	71
uncategorized	SLG (Al_2O_3 passivation layer)	PC, PV	365 nm	10^5 (estimated)	0.1	—	115
	SL-MoS_2	PC	400—680 nm	880	8	$t = 4$ s	77
	FL-WS_2	PC	457—647 nm	9.2×10^{-5}		$t = 5$ ms	81
	FL-GaS	PC	254—550 nm	0.95—19.2	2	$D = \sim 10^{10}$ (visible), $\sim 10^{14}$ (UV) Jones, $t < 30$ ms	78
	FL-GaSe	PC	254 nm	2.8	5	$t = 20$ ms	76
	FL-GaTe	PC	532 nm	10^4	5	$t = 6$ ms	80

[a] SLG, BLG, TLG: single-layer, bilayer, trilayer graphene. SL, FL: single-layer, few-layer. RT, room temperature; *D*, detectivity; *t*, response time. All the responses unspecified are data at room temperature.

CONCLUSIONS AND PERSPECTIVE

Graphene and graphene-like 2D materials have been the focus of materials science and condensed matter physics and have revealed their glamour in many fields including photodetection. Photodetection based on graphene and graphene-like 2D materials has been intensively pursued from fundamental physical mechanisms to methodologies toward improved photoresponse. We have discussed the physical mechanism including photoelectric, photo-thermoelectric, and photo-bolometric regimes, and one or more regimes could be responsible for the photoresponse in specific devices. We also carried out methodology level discussion to maximally apply these regimes to achieve high-quality photodetection and photodetectors, including both device geometry and materials engineering. By deliberately manipulating device geometry and delicate material engineering based on the profound understanding of the underneath device physics and the physical properties of 2D materials, the target to tune the photoresponse for high-performance photodetectors is approached. Many achievements have been made in ultrahigh photoresponsivity or ultrafast response speed, although it is still a challenge to have them both in a single device. The highest photoresponsivity obtained in graphene-based photodetectors is $\sim 10^7 - 10^8$ A/W at room temperature and $\sim 10^{10}$ A/W at low temperature,[71] and the ultrafast devices can be realized with a frequency as high as 500 GHz in theory.[26]

However, the large-scale, practical applications of graphene and graphene-like 2D materials in photodetection and photodetectors still have a long way to go. First, to fully exploit the extraordinary properties of graphene and graphene-like 2D materials, both discovered and undiscovered, is still a big challenge. As mentioned above, there are three or more underlying mechanisms in their photoresponse. More works are necessary to completely understand the dominating physical mechanism in various conditions and to achieve maximum performance both in photoresponsivity and response speed by device geometry tailoring and materials engineering. To achieve best response speed, photoelectric effect is the most favorable regime and PTE and photo-bolometric effects need to be suppressed. Device geometry and material modifications designed to improve the photoresponse should be selected carefully to keep the integrity of 2D materials. Severe destruction or induced defects in 2D materials will degrade the carrier mobility and the response speed. Furthermore, some newly discovered properties in graphene and graphene-like 2D materials may provide new solutions in photodetection. For example, unique properties of Dirac plasmons have been discovered in graphene recently.[53,129−141] The plasmons in graphene can have a wavelength on the order of 200 nm and can be tuned by electrostatic/chemical doping or shaping it to be micro/nanoribbon arrays in the broad terahertz frequency range.[136,137] Graphene plasmons with strong optical field confinement therefore can facilitate strong light−matter interactions, which may have a great potential to compensate the weak light absorption in graphene.

Second, coupling photonic structures with graphene has been proven to be a promising idea. Unlike other processing by chemical doping or hybrids, direct coupling of photonic structures with graphene keeps the intrinsic properties of graphene and improves the photoresponse without degradation in some desired performance such as ultrafast response speed. We note that there is still much room for improvement in materials engineering to achieve acceptable fast response speeds with ultrahigh photoresponsivity.

Third, it is very promising to explore the photodetection potential in other 2D materials beyond graphene and the heterostructures between them and graphene. Inspired by the roaring studies in graphene, many two-dimensional crystals other than graphene, such as metal chalcogenide nanosheets, are under intense study.[11−17,142] Some metal chalcogenides are semiconductors with the band gap dependent on its layer numbers and has more light absorption for specific wavelength and better wavelength selectivity than graphene. Pure metal chalcogenide nanosheets have shown a much higher photoresponsivity than pure graphene and have an acceptable response speed.[73−80] The heterostructures between metal chalcogenides and graphene have further demonstrated strong light−matter interactions.[127,128] More possibilities remain in not only photodetection but also solar energy conversion considering many unexplored semiconductor two-dimensional crystals and graphene nanocomposites.[128] Two-dimensional oxide, hydroxide, carbide, and nitride crystals are receiving more attention. Also, van der Waals heterostructures based on graphene and graphene-like 2D crystals, or based on different graphene-like 2D crystals, will be more closely investigated.[127,128,143] Both photovoltaic, photo-electrochemical, and photocatalytic applications are envisioned.[128]

Finally, we would like to mention that, beyond photonics and optoelectronics, the methodology developed here may also have great potentials in other fields like electronics, mechanical devices, electrochemistry, and biological applications.[144−153] Device geometry design and materials engineering are also two of the most important parameters for applications of 2D materials in the fields beyond photonics and optoelectronics. We believe that the emergence and maturity of 2D materials and 2D POE will inspire new insight into modern industry and find the way to large-scale applications.

Conflict of Interest: The authors declare no competing financial interest.

Acknowledgment. This work is supported by World Premier International Research Center Initiative (WPI), MEXT, Japan. H.X.C. acknowledges the funding from HUST, the WPI-AIMR fusion research funding from MEXT, and Grant-in-Aid for Young Scientists from JSPS (KAKENHI, No. 25870057), Japan. Z.H.S. acknowledges support from the ANR-2011-JS09-004-01-PvCo-Nano project.

REFERENCES AND NOTES

1. Geim, A. K.; Novoselov, K. S. The Rise of Graphene. *Nat. Mater.* **2007**, *6*, 183–191.
2. Das Sarma, S.; Adam, S.; Hwang, E. H.; Rossi, E. Electronic Transport in Two-Dimensional Graphene. *Rev. Mod. Phys.* **2011**, *83*, 407–470.
3. Dean, C. R.; Young, A. F.; Meric, I.; Lee, C.; Wang, L.; Sorgenfrei, S.; Watanabe, K.; Taniguchi, T.; Kim, P.; Shepard, K. L.; *et al.* Boron Nitride Substrates for High-Quality Graphene Electronics. *Nat. Nanotechnol.* **2010**, *5*, 722–726.
4. Schwierz, F. Graphene Transistors. *Nat. Nanotechnol.* **2010**, *5*, 487–496.
5. Meric, I.; Han, M. Y.; Young, A. F.; Ozyilmaz, B.; Kim, P.; Shepard, K. L. Current Saturation in Zero-Bandgap, Topgated Graphene Field-Effect Transistors. *Nat. Nanotechnol.* **2008**, *3*, 654–659.
6. Bonaccorso, F.; Sun, Z.; Hasan, T.; Ferrari, A. C. Graphene Photonics and Optoelectronics. *Nat. Photonics* **2010**, *4*, 611–622.
7. Lee, C.; Wei, X. D.; Kysar, J. W.; Hone, J. Measurement of the Elastic Properties and Intrinsic Strength of Monolayer Graphene. *Science* **2008**, *321*, 385–388.
8. Balandin, A. A.; Ghosh, S.; Bao, W. Z.; Calizo, I.; Teweldebrhan, D.; Miao, F.; Lau, C. N. Superior Thermal Conductivity of Single-Layer Graphene. *Nano Lett.* **2008**, *8*, 902–907.
9. Chang, H. X.; Wu, H. K. Graphene-Based Nanomaterials: Synthesis, Properties, and Optical and Optoelectronic Applications. *Adv. Funct. Mater.* **2013**, *23*, 1984–1997.
10. Chen, D.; Zhang, H.; Liu, Y.; Li, J. H. Graphene and Its Derivatives for the Development of Solar Cells, Photoelectrochemical, and Photocatalytic Applications. *Energy Environ. Sci.* **2013**, *6*, 1362–1387.
11. Radisavljevic, B.; Radenovic, A.; Brivio, J.; Giacometti, V.; Kis, A. Single-Layer MoS_2 Transistors. *Nat. Nanotechnol.* **2011**, *6*, 147–150.
12. Butler, S. Z.; Hollen, S. M.; Cao, L. Y.; Cui, Y.; Gupta, J. A.; Gutierrez, H. R.; Heinz, T. F.; Hong, S. S.; Huang, J. X.; Ismach, A. F.; *et al.* Progress, Challenges, and Opportunities in Two-Dimensional Materials Beyond Graphene. *ACS Nano* **2013**, *7*, 2898–2926.
13. Chhowalla, M.; Shin, H. S.; Eda, G.; Li, L. J.; Loh, K. P.; Zhang, H. The Chemistry of Two-Dimensional Layered Transition Metal Dichalcogenide Nanosheets. *Nat. Chem.* **2013**, *5*, 263–275.
14. Xu, M. S.; Liang, T.; Shi, M. M.; Chen, H. Z. Graphene-like Two-Dimensional Materials. *Chem. Rev.* **2013**, *113*, 3766–3798.
15. Rao, C. N. R.; Matte, H. S. S. R.; Maitra, U. Graphene Analogues of Inorganic Layered Materials. *Angew. Chem., Int. Ed.* **2013**, *52*, 13162–13185.
16. Huang, X.; Zeng, Z. Y.; Zhang, H. Metal Dichalcogenide Nanosheets: Preparation, Properties and Applications. *Chem. Soc. Rev.* **2013**, *42*, 1934–1946.
17. Zhang, X. D.; Xie, Y. Recent Advances in Free-Standing Two-Dimensional Crystals with Atomic Thickness: Design, Assembly and Transfer Strategies. *Chem. Soc. Rev.* **2013**, *42*, 8187–8199.
18. Xu, K.; Chen, P. Z.; Li, X. L.; Wu, C. Z.; Guo, Y. Q.; Zhao, J. Y.; Wu, X. J.; Xie, Y. Ultrathin Nanosheets of Vanadium Diselenide: A Metallic Two-Dimensional Material with Ferromagnetic Charge-Density-Wave Behavior. *Angew. Chem., Int. Ed.* **2013**, *52*, 10477–10481.
19. Konstantatos, G.; Sargent, E. H. Solution-Processed Quantum Dot Photodetectors. *Proc. IEEE* **2009**, *97*, 1666–1683.
20. Rogalski, A.; Antoszewski, J.; Faraone, L. Third-Generation Infrared Photodetector Arrays. *J. Appl. Phys.* **2009**, *105*, 091101.
21. Manga, K. K.; Wang, S.; Jaiswal, M.; Bao, Q. L.; Loh, K. P. High-Gain Graphene–Titanium Oxide Photoconductor Made from Inkjet Printable Ionic Solution. *Adv. Mater.* **2010**, *22*, 5265–5270.
22. Wang, Q.; Guo, X. F.; Cai, L. C.; Cao, Y.; Gan, L.; Liu, S.; Wang, Z. X.; Zhang, H. T.; Li, L. D. TiO_2-Decorated Graphenes as Efficient Photoswitches with High Oxygen Sensitivity. *Chem. Sci.* **2011**, *2*, 1860–1864.
23. Sun, Z. H.; Liu, Z. K.; Li, J. H.; Tai, G. A.; Lau, S. P.; Yan, F. Infrared Photodetectors Based on CVD-Grown Graphene and PbS Quantum Dots with Ultrahigh Responsivity. *Adv. Mater.* **2012**, *24*, 5878–5883.
24. Konstantatos, G.; Sargent, E. H. Nanostructured Materials for Photon Detection. *Nat. Nanotechnol.* **2010**, *5*, 391–400.
25. Ryzhii, V.; Ryzhii, M.; Mitin, V.; Otsuji, T. Terahertz and Infrared Photodetection Using p-i-n Multiple-Graphene-Layer Structures. *J. Appl. Phys.* **2010**, *107*, 054512.
26. Xia, F. N.; Mueller, T.; Lin, Y. M.; Valdes-Garcia, A.; Avouris, P. Ultrafast Graphene Photodetector. *Nat. Nanotechnol.* **2009**, *4*, 839–843.
27. Bao, W.; Jing, L.; Velasco, J.; Lee, Y.; Liu, G.; Tran, D.; Standley, B.; Aykol, M.; Cronin, S. B.; Smirnov, D.; *et al.* Stacking-Dependent Band Gap and Quantum Transport in Trilayer Graphene. *Nat. Phys.* **2011**, *7*, 948–952.
28. Bolotin, K. I.; Sikes, K. J.; Jiang, Z.; Klima, M.; Fudenberg, G.; Hone, J.; Kim, P.; Stormer, H. L. Ultrahigh Electron Mobility in Suspended Graphene. *Solid State Commun.* **2008**, *146*, 351–355.
29. Mueller, T.; Xia, F. N. A.; Avouris, P. Graphene Photodetectors for High-Speed Optical Communications. *Nat. Photonics* **2010**, *4*, 297–301.
30. Ohta, T.; Bostwick, A.; Seyller, T.; Horn, K.; Rotenberg, E. Controlling the Electronic Structure of Bilayer Graphene. *Science* **2006**, *313*, 951–954.
31. Chang, H. X.; Cheng, J. S.; Liu, X. Q.; Gao, J. F.; Li, M. J.; Li, J. H.; Tao, X. M.; Ding, F.; Zheng, Z. J. Facile Synthesis of Wide-Bandgap Fluorinated Graphene Semiconductors. *Chem.—Eur. J.* **2011**, *17*, 8896–8903.
32. Son, Y. W.; Cohen, M. L.; Louie, S. G. Half-Metallic Graphene Nanoribbons. *Nature* **2006**, *444*, 347–349.
33. Li, X. L.; Wang, X. R.; Zhang, L.; Lee, S. W.; Dai, H. J. Chemically Derived, Ultrasmooth Graphene Nanoribbon Semiconductors. *Science* **2008**, *319*, 1229–1232.
34. Chang, H. X.; Sun, Z. H.; Saito, M.; Yuan, Q. H.; Zhang, H.; Li, J. H.; Wang, Z. C.; Fujita, T.; Ding, F.; Zheng, Z. J.; *et al.* Regulating Infrared Photoresponses in Reduced Graphene Oxide Phototransistors by Defect and Atomic Structure Control. *ACS Nano* **2013**, *7*, 6310–6320.
35. Chang, H. X.; Sun, Z. H.; Yuan, Q. H.; Ding, F.; Tao, X. M.; Yan, F.; Zheng, Z. J. Thin Film Field-Effect Phototransistors from Bandgap-Tunable, Solution-Processed, Few-Layer Reduced Graphene Oxide Films. *Adv. Mater.* **2010**, *22*, 4872–4876.
36. Shen, Y.; Yang, S. B.; Zhou, P.; Sun, Q. Q.; Wang, P. F.; Wan, L.; Li, J.; Chen, L. Y.; Wang, X. B.; Ding, S. J.; *et al.* Evolution of the Band-Gap and Optical Properties of Graphene Oxide with Controllable Reduction Level. *Carbon* **2013**, *62*, 157–164.
37. Castro, E. V.; Novoselov, K. S.; Morozov, S. V.; Peres, N. M. R.; Dos Santos, J. M. B. L.; Nilsson, J.; Guinea, F.; Geim, A. K.; Neto, A. H. C. Biased Bilayer Graphene: Semiconductor with a Gap Tunable by the Electric Field Effect. *Phys. Rev. Lett.* **2007**, *99*, 216802.
38. Zhang, Y. B.; Tang, T. T.; Girit, C.; Hao, Z.; Martin, M. C.; Zettl, A.; Crommie, M. F.; Shen, Y. R.; Wang, F. Direct Observation of a Widely Tunable Bandgap in Bilayer Graphene. *Nature* **2009**, *459*, 820–823.
39. Shi, S. F.; Xu, X. D.; Ralph, D. C.; McEuen, P. L. Plasmon Resonance in Individual Nanogap Electrodes Studied Using Graphene Nanoconstrictions as Photodetectors. *Nano Lett.* **2011**, *11*, 1814–1818.

40. Echtermeyer, T. J.; Britnell, L.; Jasnos, P. K.; Lombardo, A.; Gorbachev, R. V.; Grigorenko, A. N.; Geim, A. K.; Ferrari, A. C.; Novoselov, K. S. Strong Plasmonic Enhancement of Photovoltage in Graphene. *Nat. Commun.* **2011**, *2*, 458.
41. Liu, Y.; Cheng, R.; Liao, L.; Zhou, H. L.; Bai, J. W.; Liu, G.; Liu, L. X.; Huang, Y.; Duan, X. F. Plasmon Resonance Enhanced Multicolour Photodetection by Graphene. *Nat. Commun.* **2011**, *2*, 579.
42. Gao, W. L.; Shu, J.; Qiu, C. Y.; Xu, Q. F. Excitation of Plasmonic Waves in Graphene by Guided-Mode Resonances. *ACS Nano* **2012**, *6*, 7806–7813.
43. Nie, B. A.; Hu, J. G.; Luo, L. B.; Xie, C.; Zeng, L. H.; Lv, P.; Li, F. Z.; Jie, J. S.; Feng, M.; Wu, C. Y.; *et al.* Monolayer Graphene Film on ZnO Nanorod Array for High-Performance Schottky Junction Ultraviolet Photodetectors. *Small* **2013**, *9*, 2872–2879.
44. Liu, M.; Yin, X. B.; Ulin-Avila, E.; Geng, B. S.; Zentgraf, T.; Ju, L.; Wang, F.; Zhang, X. A Graphene-Based Broadband Optical Modulator. *Nature* **2011**, *474*, 64–67.
45. Kim, K.; Choi, J. Y.; Kim, T.; Cho, S. H.; Chung, H. J. A Role for Graphene in Silicon-Based Semiconductor Devices. *Nature* **2011**, *479*, 338–344.
46. Gan, X. T.; Shiue, R. J.; Gao, Y. D.; Meric, I.; Heinz, T. F.; Shepard, K.; Hone, J.; Assefa, S.; Englund, D. Chip-Integrated Ultrafast Graphene Photodetector with High Responsivity. *Nat. Photonics* **2013**, *7*, 883–887.
47. Pospischil, A.; Humer, M.; Furchi, M. M.; Bachmann, D.; Guider, R.; Fromherz, T.; Mueller, T. CMOS-Compatible Graphene Photodetector Covering All Optical Communication Bands. *Nat. Photonics* **2013**, *7*, 892–896.
48. Wang, X. M.; Cheng, Z. Z.; Xu, K.; Tsang, H. K.; Xu, J. B. High-Responsivity Graphene/Silicon-Heterostructure Waveguide Photodetectors. *Nat. Photonics* **2013**, *7*, 888–891.
49. Ferreira, A.; Peres, N. M. R.; Ribeiro, R. M.; Stauber, T. Graphene-Based Photodetector with Two Cavities. *Phys. Rev. B* **2012**, *85*, 115438.
50. Furchi, M.; Urich, A.; Pospischil, A.; Lilley, G.; Unterrainer, K.; Detz, H.; Klang, P.; Andrews, A. M.; Schrenk, W.; Strasser, G.; *et al.* Microcavity-Integrated Graphene Photodetector. *Nano Lett.* **2012**, *12*, 2773–2777.
51. Engel, M.; Steiner, M.; Lombardo, A.; Ferrari, A. C.; Lohneysen, H. V.; Avouris, P.; Krupke, R. Light–Matter Interaction in a Microcavity-Controlled Graphene Transistor. *Nat. Commun.* **2012**, *3*, 906.
52. Gan, X. T.; Mak, K. F.; Gao, Y. D.; You, Y. M.; Hatami, F.; Hone, J.; Heinz, T. F.; Englund, D. Strong Enhancement of Light–Matter Interaction in Graphene Coupled to a Photonic Crystal Nanocavity. *Nano Lett.* **2012**, *12*, 5626–5631.
53. Grigorenko, A. N.; Polini, M.; Novoselov, K. S. Graphene Plasmonics. *Nat. Photonics* **2012**, *6*, 749–758.
54. Cao, A. N.; Liu, Z.; Chu, S. S.; Wu, M. H.; Ye, Z. M.; Cai, Z. W.; Chang, Y. L.; Wang, S. F.; Gong, Q. H.; Liu, Y. F. A Facile One-Step Method To Produce Graphene–CdS Quantum Dot Nanocomposites as Promising Optoelectronic Materials. *Adv. Mater.* **2010**, *22*, 103–106.
55. Manga, K. K.; Zhou, Y.; Yan, Y. L.; Loh, K. P. Multilayer Hybrid Films Consisting of Alternating Graphene and Titania Nanosheets with Ultrafast Electron Transfer and Photoconversion Properties. *Adv. Funct. Mater.* **2009**, *19*, 3638–3643.
56. Geng, X. M.; Niu, L.; Xing, Z. Y.; Song, R. S.; Liu, G. T.; Sun, M. T.; Cheng, G. S.; Zhong, H. J.; Liu, Z. H.; Zhang, Z. J.; *et al.* Aqueous-Processable Noncovalent Chemically Converted Graphene–Quantum Dot Composites for Flexible and Transparent Optoelectronic Films. *Adv. Mater.* **2010**, *22*, 638–642.
57. Shi, Y. M.; Fang, W. J.; Zhang, K. K.; Zhang, W. J.; Li, L. J. Photoelectrical Response in Single-Layer Graphene Transistors. *Small* **2009**, *5*, 2005–2011.
58. Chang, H. X.; Sun, Z. H.; Ho, K. Y. F.; Tao, X. M.; Yan, F.; Kwok, W. M.; Zheng, Z. J. A Highly Sensitive Ultraviolet Sensor Based on a Facile *In Situ* Solution-Grown ZnO Nanorod/Graphene Heterostructure. *Nanoscale* **2011**, *3*, 258–264.
59. Chang, H. X.; Lv, X. J.; Zhang, H.; Li, J. H. Quantum Dots Sensitized Graphene: *In Situ* Growth and Application in Photoelectrochemical Cells. *Electrochem. Commun.* **2010**, *12*, 483–487.
60. Zhang, D. Y.; Gan, L.; Cao, Y.; Wang, Q.; Qi, L. M.; Guo, X. F. Understanding Charge Transfer at PbS-Decorated Graphene Surfaces toward a Tunable Photosensor. *Adv. Mater.* **2012**, *24*, 2715–2720.
61. Konstantatos, G.; Badioli, M.; Gaudreau, L.; Osmond, J.; Bernechea, M.; de Arquer, F. P. G.; Gatti, F.; Koppens, F. H. L. Hybrid Graphene-Quantum Dot Phototransistors with Ultrahigh Gain. *Nat. Nanotechnol.* **2012**, *7*, 363–368.
62. Jeon, E. K.; Yang, C. S.; Shen, Y. F.; Nakanishi, T.; Jeong, D. S.; Kim, J. J.; Ahn, K. S.; Kong, K. J.; Lee, J. O. Photoconductivity and Enhanced Memory Effects in Hybrid C_{60}-Graphene Transistors. *Nanotechnology* **2012**, *23*, 455202.
63. Son, D. I.; Yang, H. Y.; Kim, T. W.; Park, W. I. Photoresponse Mechanisms of Ultraviolet Photodetectors Based on Colloidal ZnO Quantum Dot–Graphene Nanocomposites. *Appl. Phys. Lett.* **2013**, *102*, 021105.
64. An, X. H.; Liu, F. Z.; Jung, Y. J.; Kar, S. Tunable Graphene–Silicon Heterojunctions for Ultrasensitive Photodetection. *Nano Lett.* **2013**, *13*, 909–916.
65. Chen, S. Y.; Lu, Y. Y.; Shih, F. Y.; Ho, P. H.; Chen, Y. F.; Chen, C. W.; Chen, Y. T.; Wang, W. H. Biologically Inspired Graphene-Chlorophyll Phototransistors with High Gain. *Carbon* **2013**, *63*, 23–29.
66. Cheng, S. H.; Weng, T. M.; Lu, M. L.; Tan, W. C.; Chen, J. Y.; Chen, Y. F. All Carbon-Based Photodetectors: An Eminent Integration of Graphite Quantum Dots and Two Dimensional Graphene. *Sci. Rep.* **2013**, *3*, 2694.
67. Roy, K.; Padmanabhan, M.; Goswami, S.; Phanindra Sai, T.; Kaushal, S.; Ghosh, A. Optically Active Heterostructures of Graphene and Ultra Thin MoS_2. *Solid State Commun.* **2013**, *175–176*, 35–42.
68. Zhang, W.; Chuu, C.-P.; Huang, J.-K.; Chen, C.-H.; Tsai, M.-L.; Chang, Y.-H.; Liang, C.-T.; He, J.-H.; Chou, M.-Y.; Li, L.-J. Ultrahigh-Gain Phototransistors Based on Atomically Thin Graphene–MoS_2 Heterostructures. *Sci. Rep.* **2014**, *4*, 3826.
69. Guo, W. H.; Xu, S. G.; Wu, Z. F.; Wang, N.; Loy, M. M. T.; Du, S. W. Oxygen-Assisted Charge Transfer between ZnO Quantum Dots and Graphene. *Small* **2013**, *9*, 3031–3036.
70. Huang, Y. Q.; Zhu, R. J.; Kang, N.; Du, J.; Xu, H. Q. Photoelectrical Response of Hybrid Graphene–PbS Quantum Dot Devices. *Appl. Phys. Lett.* **2013**, *103*, 143119.
71. Roy, K.; Padmanabhan, M.; Goswami, S.; Sai, T. P.; Ramalingam, G.; Raghavan, S.; Ghosh, A. Graphene–MoS_2 Hybrid Structures for Multifunctional Photoresponsive Memory Devices. *Nat. Nanotechnol.* **2013**, *8*, 826–830.
72. Buscema, M.; Barkelid, M.; Zwiller, V.; van der Zant, H. S. J.; Steele, G. A.; Castellanos-Gomez, A. Large and Tunable Photothermoelectric Effect in Single-Layer MoS_2. *Nano Lett.* **2013**, *13*, 358–363.
73. Yin, Z. Y.; Li, H.; Li, H.; Jiang, L.; Shi, Y. M.; Sun, Y. H.; Lu, G.; Zhang, Q.; Chen, X. D.; Zhang, H. Single-Layer MoS_2 Phototransistors. *ACS Nano* **2012**, *6*, 74–80.
74. Choi, W.; Cho, M. Y.; Konar, A.; Lee, J. H.; Cha, G. B.; Hong, S. C.; Kim, S.; Kim, J.; Jena, D.; Joo, J.; *et al.* High-Detectivity Multilayer MoS_2 Phototransistors with Spectral Response from Ultraviolet to Infrared. *Adv. Mater.* **2012**, *24*, 5832–5836.
75. Lee, H. S.; Min, S. W.; Chang, Y. G.; Park, M. K.; Nam, T.; Kim, H.; Kim, J. H.; Ryu, S.; Im, S. MoS_2 Nanosheet Phototransistors with Thickness-Modulated Optical Energy Gap. *Nano Lett.* **2012**, *12*, 3695–3700.
76. Hu, P. A.; Wen, Z. Z.; Wang, L. F.; Tan, P. H.; Xiao, K. Synthesis of Few-Layer GaSe Nanosheets for High Performance Photodetectors. *ACS Nano* **2012**, *6*, 5988–5994.
77. Lopez-Sanchez, O.; Lembke, D.; Kayci, M.; Radenovic, A.; Kis, A. Ultrasensitive Photodetectors Based on Monolayer MoS_2. *Nat. Nanotechnol.* **2013**, *8*, 497–501.

78. Hu, P. A.; Wang, L. F.; Yoon, M.; Zhang, J.; Feng, W.; Wang, X. N.; Wen, Z. Z.; Idrobo, J. C.; Miyamoto, Y.; Geohegan, D. B.; *et al.* Highly Responsive Ultrathin GaS Nanosheet Photodetectors on Rigid and Flexible Substrates. *Nano Lett.* **2013**, *13*, 1649–1654.
79. Zhang, W. J.; Huang, J. K.; Chen, C. H.; Chang, Y. H.; Cheng, Y. J.; Li, L. J. High-Gain Phototransistors Based on a CVD MoS_2 Monolayer. *Adv. Mater.* **2013**, *25*, 3456–3461.
80. Liu, F.; Shimotani, H.; Shang, H.; Kanagasekaran, T.; Zólyomi, V.; Drummond, N.; Fal'ko, V. I.; Tanigaki, K. High-Sensitivity Photodetectors Based on Multilayer GaTe Flakes. *ACS Nano* **2014**, *8*, 752–760.
81. Perea-Lopez, N.; Elias, A. L.; Berkdemir, A.; Castro-Beltran, A.; Gutierrez, H. R.; Feng, S. M.; Lv, R. T.; Hayashi, T.; Lopez-Urias, F.; Ghosh, S.; *et al.* Photosensor Device Based on Few-Layered WS_2 Films. *Adv. Funct. Mater.* **2013**, *23*, 5511–5517.
82. Lei, S. D.; Ge, L. H.; Liu, Z.; Najmaei, S.; Shi, G.; You, G.; Lou, J.; Vajtai, R.; Ajayan, P. M. Synthesis and Photoresponse of Large GaSe Atomic Layers. *Nano Lett.* **2013**, *13*, 2777–2781.
83. Lee, E. J. H.; Balasubramanian, K.; Weitz, R. T.; Burghard, M.; Kern, K. Contact and Edge Effects in Graphene Devices. *Nat. Nanotechnol.* **2008**, *3*, 486–490.
84. Xia, F. N.; Mueller, T.; Golizadeh-Mojarad, R.; Freitag, M.; Lin, Y. M.; Tsang, J.; Perebeinos, V.; Avouris, P. Photocurrent Imaging and Efficient Photon Detection in a Graphene Transistor. *Nano Lett.* **2009**, *9*, 1039–1044.
85. Park, J.; Ahn, Y. H.; Ruiz-Vargas, C. Imaging of Photocurrent Generation and Collection in Single-Layer Graphene. *Nano Lett.* **2009**, *9*, 1742–1746.
86. Mueller, T.; Xia, F.; Freitag, M.; Tsang, J.; Avouris, P. Role of Contacts in Graphene Transistors: A Scanning Photocurrent Study. *Phys. Rev. B* **2009**, *79*, 245430.
87. Peters, E. C.; Lee, E. J. H.; Burghard, M.; Kern, K. Gate Dependent Photocurrents at a Graphene p-n Junction. *Appl. Phys. Lett.* **2010**, *97*, 193102.
88. Urich, A.; Unterrainer, K.; Mueller, T. Intrinsic Response Time of Graphene Photodetectors. *Nano Lett.* **2011**, *11*, 2804–2808.
89. Prechtel, L.; Song, L.; Schuh, D.; Ajayan, P.; Wegscheider, W.; Holleitner, A. W. Time-Resolved Ultrafast Photocurrents and Terahertz Generation in Freely Suspended Graphene. *Nat. Commun.* **2012**, *3*, 646.
90. Xu, X. D.; Gabor, N. M.; Alden, J. S.; van der Zande, A. M.; McEuen, P. L. Photo-thermoelectric Effect at a Graphene Interface Junction. *Nano Lett.* **2010**, *10*, 562–566.
91. Song, J. C. W.; Rudner, M. S.; Marcus, C. M.; Levitov, L. S. Hot Carrier Transport and Photocurrent Response in Graphene. *Nano Lett.* **2011**, *11*, 4688–4692.
92. Gabor, N. M.; Song, J. C. W.; Ma, Q.; Nair, N. L.; Taychatanapat, T.; Watanabe, K.; Taniguchi, T.; Levitov, L. S.; Jarillo-Herrero, P. Hot Carrier-Assisted Intrinsic Photoresponse in Graphene. *Science* **2011**, *334*, 648–652.
93. Hsieh, C. Y.; Chen, Y. T.; Tan, W. J.; Chen, Y. F.; Shih, W. Y.; Shih, W. H. Graphene-Lead Zirconate Titanate Optothermal Field Effect Transistors. *Appl. Phys. Lett.* **2012**, *100*, 113507.
94. Tielrooij, K. J.; Song, J. C. W.; Jensen, S. A.; Centeno, A.; Pesquera, A.; Elorza, A. Z.; Bonn, M.; Levitov, L. S.; Koppens, F. H. L. Photoexcitation Cascade and Multiple Hot-Carrier Generation in Graphene. *Nat. Phys.* **2013**, *9*, 248–252.
95. Freitag, M.; Low, T.; Avouris, P. Increased Responsivity of Suspended Graphene Photodetectors. *Nano Lett.* **2013**, *13*, 1644–1648.
96. Patil, V.; Capone, A.; Strauf, S.; Yang, E. H. Improved Photoresponse with Enhanced Photoelectric Contribution in Fully Suspended Graphene Photodetectors. *Sci. Rep.* **2013**, *3*, 2791.
97. Lemme, M. C.; Koppens, F. H. L.; Falk, A. L.; Rudner, M. S.; Park, H.; Levitov, L. S.; Marcus, C. M. Gate-Activated Photoresponse in a Graphene p-n Junction. *Nano Lett.* **2011**, *11*, 4134–4137.
98. Vora, H.; Kumaravadivel, P.; Nielsen, B.; Du, X. Bolometric Response in Graphene Based Superconducting Tunnel Junctions. *Appl. Phys. Lett.* **2012**, *100*, 153507.
99. Yan, J.; Kim, M. H.; Elle, J. A.; Sushkov, A. B.; Jenkins, G. S.; Milchberg, H. M.; Fuhrer, M. S.; Drew, H. D. Dual-Gated Bilayer Graphene Hot-Electron Bolometer. *Nat. Nanotechnol.* **2012**, *7*, 472–478.
100. Freitag, M.; Low, T.; Xia, F. N.; Avouris, P. Photoconductivity of Biased Graphene. *Nat. Photonics* **2013**, *7*, 53–59.
101. Kim, M. H.; Yan, J.; Suess, R. J.; Murphy, T. E.; Fuhrer, M. S.; Drew, H. D. Photothermal Response in Dual-Gated Bilayer Graphene. *Phys. Rev. Lett.* **2013**, *110*, 247402.
102. Sun, D.; Wu, Z. K.; Divin, C.; Li, X. B.; Berger, C.; de Heer, W. A.; First, P. N.; Norris, T. B. Ultrafast Relaxation of Excited Dirac Fermions in Epitaxial Graphene Using Optical Differential Transmission Spectroscopy. *Phys. Rev. Lett.* **2008**, *101*, 157402.
103. Dawlaty, J. M.; Shivaraman, S.; Chandrashekhar, M.; Rana, F.; Spencer, M. G. Measurement of Ultrafast Carrier Dynamics in Epitaxial Graphene. *Appl. Phys. Lett.* **2008**, *92*, 042116.
104. Giovannetti, G.; Khomyakov, P. A.; Brocks, G.; Karpan, V. M.; van den Brink, J.; Kelly, P. J. Doping Graphene with Metal Contacts. *Phys. Rev. Lett.* **2008**, *101*, 026803.
105. Bistritzer, R.; MacDonald, A. H. Electronic Cooling in Graphene. *Phys. Rev. Lett.* **2009**, *102*, 206410.
106. Wei, P.; Bao, W. Z.; Pu, Y.; Lau, C. N.; Shi, J. Anomalous Thermoelectric Transport of Dirac Particles in Graphene. *Phys. Rev. Lett.* **2009**, *102*, 166808.
107. Zuev, Y. M.; Chang, W.; Kim, P. Thermoelectric and Magnetothermoelectric Transport Measurements of Graphene. *Phys. Rev. Lett.* **2009**, *102*, 096807.
108. Checkelsky, J. G.; Ong, N. P. Thermopower and Nernst Effect in Graphene in a Magnetic Field. *Phys. Rev. B* **2009**, *80*, 081413.
109. Stutzel, E. U.; Dufaux, T.; Sagar, A.; Rauschenbach, S.; Balasubramanian, K.; Burghard, M.; Kern, K. Spatially Resolved Photocurrents in Graphene Nanoribbon Devices. *Appl. Phys. Lett.* **2013**, *102*, 043106.
110. Ryzhii, V.; Mitin, V.; Ryzhii, M.; Ryabova, N.; Otsuji, T. Device Model for Graphene Nanoribbon Phototransistor. *Appl. Phys. Express* **2008**, *1*, 063002.
111. Ryzhii, V.; Ryzhii, M.; Ryabova, N.; Mitin, V.; Otsuji, T. Graphene Nanoribbon Phototransistor: Proposal and Analysis. *Jpn. J. Appl. Phys.* **2009**, *48*, 04C144.
112. Han, M. Y.; Ozyilmaz, B.; Zhang, Y. B.; Kim, P. Energy Band-Gap Engineering of Graphene Nanoribbons. *Phys. Rev. Lett.* **2007**, *98*, 206805.
113. Ryzhii, V.; Ryzhii, M. Graphene Bilayer Field-Effect Phototransistor for Terahertz and Infrared Detection. *Phys. Rev. B* **2009**, *79*, 245311.
114. Ryzhii, V.; Ryzhii, M.; Ryabova, N.; Mitin, V.; Otsuji, T. Terahertz and Infrared Detectors Based on Graphene Structures. *Infrared Phys. Technol.* **2011**, *54*, 302–305.
115. Kang, C. G.; Lee, S. K.; Choe, S. H.; Lee, Y. G.; Lee, C. L.; Lee, B. H. Intrinsic Photocurrent Characteristics of Graphene Photodetectors Passivated with Al_2O_3. *Opt. Express* **2013**, *21*, 23391–23400.
116. Son, Y. W.; Cohen, M. L.; Louie, S. G. Energy Gaps in Graphene Nanoribbons. *Phys. Rev. Lett.* **2006**, *97*, 216803.
117. Chen, Z. H.; Lin, Y. M.; Rooks, M. J.; Avouris, P. Graphene Nano-Ribbon Electronics. *Physica E* **2007**, *40*, 228–232.
118. Liao, A. D.; Wu, J. Z.; Wang, X. R.; Tahy, K.; Jena, D.; Dai, H. J.; Pop, E. Thermally Limited Current Carrying Ability of Graphene Nanoribbons. *Phys. Rev. Lett.* **2011**, *106*, 256801.
119. Chitara, B.; Panchakarla, L. S.; Krupanidhi, S. B.; Rao, C. N. R. Infrared Photodetectors Based on Reduced Graphene Oxide and Graphene Nanoribbons. *Adv. Mater.* **2011**, *23*, 5419–5424.
120. Freitag, M.; Low, T.; Zhu, W. J.; Yan, H. G.; Xia, F. N.; Avouris, P. Photocurrent in Graphene Harnessed by Tunable Intrinsic Plasmons. *Nat. Commun.* **2013**, *4*, 1951.
121. Zhang, Y. Z.; Liu, T.; Meng, B.; Li, X. H.; Liang, G. Z.; Hu, X. N.; Wang, Q. J. Broadband High Photoresponse from Pure Monolayer Graphene Photodetector. *Nat. Commun.* **2013**, *4*, 1811.
122. Farmer, D. B.; Golizadeh-Mojarad, R.; Perebeinos, V.; Lin, Y. M.; Tulevski, G. S.; Tsang, J. C.; Avouris, P. Chemical Doping and Electron–Hole Conduction Asymmetry in Graphene Devices. *Nano Lett.* **2009**, *9*, 388–392.

123. Farmer, D. B.; Lin, Y. M.; Afzali-Ardakani, A.; Avouris, P. Behavior of a Chemically Doped Graphene Junction. *Appl. Phys. Lett.* **2009**, *94*, 213106.
124. Yan, H. G.; Xia, F. N.; Zhu, W. J.; Freitag, M.; Dimitrakopoulos, C.; Bol, A. A.; Tulevski, G.; Avouris, P. Infrared Spectroscopy of Wafer-Scale Graphene. *ACS Nano* **2011**, *5*, 9854–9860.
125. Chitara, B.; Krupanidhi, S. B.; Rao, C. N. R. Solution Processed Reduced Graphene Oxide Ultraviolet Detector. *Appl. Phys. Lett.* **2011**, *99*, 113114.
126. Kurra, N.; Bhadram, V. S.; Narayana, C.; Kulkarni, G. U. Few Layer Graphene to Graphitic Films: Infrared Photoconductive *versus* Bolometric Response. *Nanoscale* **2013**, *5*, 381–389.
127. Britnell, L.; Ribeiro, R. M.; Eckmann, A.; Jalil, R.; Belle, B. D.; Mishchenko, A.; Kim, Y. J.; Gorbachev, R. V.; Georgiou, T.; Morozov, S. V.; *et al.* Strong Light−Matter Interactions in Heterostructures of Atomically Thin Films. *Science* **2013**, *340*, 1311–1314.
128. Chang, H. X.; Wu, H. K. Graphene-Based Nanocomposites: Preparation, Functionalization, and Energy and Environmental Applications. *Energy Environ. Sci.* **2013**, *6*, 3483–3507.
129. Hwang, E. H.; Das Sarma, S. Dielectric Function, Screening, and Plasmons in Two-Dimensional Graphene. *Phys. Rev. B* **2007**, *75*, 205418.
130. Jablan, M.; Buljan, H.; Soljacic, M. Plasmonics in Graphene at Infrared Frequencies. *Phys. Rev. B* **2009**, *80*, 245435.
131. Ju, L.; Geng, B. S.; Horng, J.; Girit, C.; Martin, M.; Hao, Z.; Bechtel, H. A.; Liang, X. G.; Zettl, A.; Shen, Y. R.; *et al.* Graphene Plasmonics for Tunable Terahertz Metamaterials. *Nat. Nanotechnol.* **2011**, *6*, 630–634.
132. Jablan, M.; Soljacic, M.; Buljan, H. Unconventional Plasmon−Phonon Coupling in Graphene. *Phys. Rev. B* **2011**, *83*, 161409.
133. Koppens, F. H. L.; Chang, D. E.; de Abajo, F. J. G. Graphene Plasmonics: A Platform for Strong Light−Matter Interactions. *Nano Lett.* **2011**, *11*, 3370–3377.
134. Fei, Z.; Andreev, G. O.; Bao, W. Z.; Zhang, L. F. M.; McLeod, A. S.; Wang, C.; Stewart, M. K.; Zhao, Z.; Dominguez, G.; Thiemens, M.; *et al.* Infrared Nanoscopy of Dirac Plasmons at the Graphene−SiO_2 Interface. *Nano Lett.* **2011**, *11*, 4701–4705.
135. Shin, S. Y.; Kim, N. D.; Kim, J. G.; Kim, K. S.; Noh, D. Y.; Kim, K. S.; Chung, J. W. Control of the π Plasmon in a Single Layer Graphene by Charge Doping. *Appl. Phys. Lett.* **2011**, *99*, 082110.
136. Chen, J. N.; Badioli, M.; Alonso-Gonzalez, P.; Thongrattanasiri, S.; Huth, F.; Osmond, J.; Spasenovic, M.; Centeno, A.; Pesquera, A.; Godignon, P.; *et al.* Optical Nano-Imaging of Gate-Tunable Graphene Plasmons. *Nature* **2012**, *487*, 77–81.
137. Fei, Z.; Rodin, A. S.; Andreev, G. O.; Bao, W.; McLeod, A. S.; Wagner, M.; Zhang, L. M.; Zhao, Z.; Thiemens, M.; Dominguez, G.; *et al.* Gate-Tuning of Graphene Plasmons Revealed by Infrared Nano-Imaging. *Nature* **2012**, *487*, 82–85.
138. Crassee, I.; Orlita, M.; Potemski, M.; Walter, A. L.; Ostler, M.; Seyller, T.; Gaponenko, I.; Chen, J.; Kuzmenko, A. B. Intrinsic Terahertz Plasmons and Magnetoplasmons in Large Scale Monolayer Graphene. *Nano Lett.* **2012**, *12*, 2470–2474.
139. Bao, Q. L.; Loh, K. P. Graphene Photonics, Plasmonics, and Broadband Optoelectronic Devices. *ACS Nano* **2012**, *6*, 3677–3694.
140. Thongrattanasiri, S.; Manjavacas, A.; de Abajo, F. J. G. Quantum Finite-Size Effects in Graphene Plasmons. *ACS Nano* **2012**, *6*, 1766–1775.
141. Fang, Z. Y.; Thongrattanasiri, S.; Schlather, A.; Liu, Z.; Ma, L. L.; Wang, Y. M.; Ajayan, P. M.; Nordlander, P.; Halas, N. J.; de Abajo, F. J. G. Gated Tunability and Hybridization of Localized Plasmons in Nanostructured Graphene. *ACS Nano* **2013**, *7*, 2388–2395.
142. Coleman, J. N.; Lotya, M.; O'Neill, A.; Bergin, S. D.; King, P. J.; Khan, U.; Young, K.; Gaucher, A.; De, S.; Smith, R. J.; *et al.* Two-Dimensional Nanosheets Produced by Liquid Exfoliation of Layered Materials. *Science* **2011**, *331*, 568–571.
143. Geim, A. K.; Grigorieva, I. V. van der Waals Heterostructures. *Nature* **2013**, *499*, 419–425.
144. Wang, Q. H.; Kalantar-Zadeh, K.; Kis, A.; Coleman, J. N.; Strano, M. S. Electronics and Optoelectronics of Two-Dimensional Transition Metal Dichalcogenides. *Nat. Nanotechnol.* **2012**, *7*, 699–712.
145. Du, X.; Skachko, I.; Barker, A.; Andrei, E. Y. Approaching Ballistic Transport in Suspended Graphene. *Nat. Nanotechnol.* **2008**, *3*, 491–495.
146. Britnell, L.; Gorbachev, R. V.; Jalil, R.; Belle, B. D.; Schedin, F.; Mishchenko, A.; Georgiou, T.; Katsnelson, M. I.; Eaves, L.; Morozov, S. V.; *et al.* Field-Effect Tunneling Transistor Based on Vertical Graphene Heterostructures. *Science* **2012**, *335*, 947–950.
147. Bunch, J. S.; van der Zande, A. M.; Verbridge, S. S.; Frank, I. W.; Tanenbaum, D. M.; Parpia, J. M.; Craighead, H. G.; McEuen, P. L. Electromechanical Resonators from Graphene Sheets. *Science* **2007**, *315*, 490–493.
148. Chen, D.; Feng, H. B.; Li, J. H. Graphene Oxide: Preparation, Functionalization, and Electrochemical Applications. *Chem. Rev.* **2012**, *112*, 6027–6053.
149. Pumera, M. Graphene-Based Nanomaterials and Their Electrochemistry. *Chem. Soc. Rev.* **2010**, *39*, 4146–4157.
150. Chen, D.; Tang, L. H.; Li, J. H. Graphene-Based Materials in Electrochemistry. *Chem. Soc. Rev.* **2010**, *39*, 3157–3180.
151. Liu, Y. X.; Dong, X. C.; Chen, P. Biological and Chemical Sensors Based on Graphene Materials. *Chem. Soc. Rev.* **2012**, *41*, 2283–2307.
152. Shi, X. T.; Chang, H. X.; Chen, S.; Lai, C.; Khademhosseini, A.; Wu, H. K. Regulating Cellular Behavior on Few-Layer Reduced Graphene Oxide Films with Well-Controlled Reduction States. *Adv. Funct. Mater.* **2012**, *22*, 751–759.
153. Yang, K.; Feng, L. Z.; Shi, X. Z.; Liu, Z. Nano-Graphene in Biomedicine: Theranostic Applications. *Chem. Soc. Rev.* **2013**, *42*, 530–547.